Integrated Sled Testing, Computer Modeling, and Scientific Visualization for Crashworthy Child Restraint System Design

Robert A. Galganski,[1] **Ioannis Hatziprokopiou**
General Dynamics[2]
4455 Genesee Street, Buffalo, NY 14225
robert.galganski@gd-ais.com; ioannis.hatziprokopiou@gd-ais.com
716-631-6892 [fax: 6843]; 716-632-7500 (x5503) [fax: 6843]

Kevin F. Hulme
University at Buffalo
New York State Center for Engineering Design and Industrial Innovation
5 Norton Hall
Buffalo, NY 14260-1810
hulme@buffalo.edu
716-645-2685 (x103) [fax: 2684]

Abani Patra, Nataraju Vusirikala
University at Buffalo
Department of Mechanical and Aerospace Engineering
605 Furnas Hall; 804 Furnas Hall
Buffalo, NY 14260-4400
abani@eng.buffalo.edu; nv5@eng.buffalo.edu
716-645-2593 (x2240) [fax: 3875]; 716-645-2593 (x2239) [fax: 3875]

ABSTRACT

A recent study examined the use of virtual reality imagery in conjunction with MADYMO computational modeling to facilitate prototype development and existing-design optimization of crashworthy child restraint systems (CRS). A postprocessing tool called NCVM (NYSCEDII CRS Visualization Module) was developed as part of that research. It enables scientists and engineers to view selected MADYMO imagery with a sense of depth and immersion while analyzing computer-forecasted CRS deformations and loadings.

The purpose of this paper is twofold. The first describes our efforts to predict strains induced on the surface of a CRS shell structure subjected to a modified FMVSS 213 sled test environment using an appropriate MADYMO model. These forecasts are compared with their empirical counterparts obtained from a series of modified FMVSS 213 sled tests. "What-if" studies are also conducted with a validated model to explore its potential for use as a sled-test planning tool.

The development and design of planned new features for the next NCVM upgrade is also detailed. They include (1) a volumetric "slicing" capability that allows MADYMO users to

[1] Corresponding author.
[2] Funding for this effort was provided by the Federal Highway Administration (FHWA) through the Calspan-UB Research Center, Inc. (CUBRC) Center for Transportation Injury Research Project.

observe computer animations of simulated CRS and dummy interaction and other responses inside a virtual vehicle cabin; (2) a "vapor trails" feature that tracks occupant displacement over the entire simulation duration on a single screen frame; and (3) additional user-specified viewing options that permit CRS/dummy models to be visualized from commonly used "hot views." These visual vantage points correspond directly with camera placement views commonly employed during an actual sled test experiment.

INTRODUCTION

New child restraint system (CRS) designs are generally developed in a cyclic, build-and-test fashion. The initial conceptual design is fabricated and subjected to a sled test delineated in a rigorous test procedure as defined in the applicable government safety regulation (in the U.S., test procedure [1] is specified by Federal Motor Vehicle Safety Standard (FMVSS) 213 [2]). CRS safety performance is evaluated by comparing the relevant electronic data and other observations obtained from the test relative to occupant injury criteria defined in that standard. In most cases, the initial design does not comply with all requirements and one or more alterations must be made to the system, leading to the fabrication of a second prototype and another sled test. This cycle may continue if necessary—culminating with a final design when (at least) the mandated minimum safety requirements are met.

Total reliance on such testing-driven product development can become cost prohibitive if it continues for too long (the same reasoning applies to the case of a manufacturer seeking to optimize an existing compliant design). This is particularly true for consumer products such as a CRS, where aesthetics are an important sales consideration. Researchers have long posited that the number of such cycles could be shortened—perhaps substantially—by supplementing this traditional approach with the judicious use of validated and reliable computational modeling. For example, extensive "what-if?" exploratory studies could be conducted at critical stages of the process to provide much-needed guidance to help select at least the general direction a design change should take.

It should be noted, however, that the use of modeling for this purpose is itself a complex (and contentious) issue. Indeed, Committee No. 60 of the American Society of Mechanical Engineers is currently working toward developing international standards governing the correctness and credibility of all modeling and simulation activities [3]. When completed, currently bandied-about terms such as model "validation" will at last be subject to strict protocols (see, e.g., [4] and [5]). We will document in this paper a systematic process of model development and testing to validate a series of CRS models.

The Center for Transportation Industry Research (CenTIR)[3] recently took a fresh look at the potential benefits that computational modeling could offer crashworthy CRS design. Our initial

[3] The Center for Transportation Injury Research (CenTIR) is a Calspan-UB Research Center, Inc. (CUBRC)-led team that performs interdisciplinary, systems-oriented research to reduce the occurrence, severity, and consequences of crash-related injuries. The team includes the Buffalo, New York, facility of General Dynamics Advanced Information Engineering Services (formerly Veridian Engineering); the University at Buffalo, School of Engineering and Applied Sciences and the Department of Emergency Medicine; and the Erie County Medical Center (Level 1 Trauma Center).

endeavor [6] focused on developing a combination rigid body and finite element model of a oduction CRS using the well-known MADYMO (MAthematical DYnamical MOdels) code [7]. The resulting "validated" model reflected the end product of a series of systematic enhancements until the model provided satisfactory correlation between experimental and simulation results. As such, the range of FMVSS 213 dummy body segment displacement and acceleration responses measured in two series of repetitive sled tests were regarded as "definitive."

The results documented in this paper were generated by an upgraded MADYMO model that can predict strain experienced in a CRS shell subjected to the above-mentioned dynamic loading. Accordingly, model validation was extended to include this arguably most crucial *structural* response parameter involved in CRS shell design. The paper also explores the possibility of using the new model to provide insight and guidance during developmental sled testing to facilitate the critical placement of strain gage sensors on the shell.

The initial CenTIR study also examined the feasibility of using virtual reality (VR) to enhance analyses of MADYMO output imagery and critically support the design process by providing a realistic "look and feel" to analysis results. This effort culminated in the development of a postprocessing utility called NCVM (NYSCEDII CRS Visualization Module). The NCVM allows the MADYMO user to observe three-dimensional geometries depicting the displacement of a CRS/dummy configuration in a simulated modified FMVSS 213 crash environment. The immersive, stereoscopic simulation integrates relevant engineering crash test data (stress and acceleration) with displaced model geometries during the simulated crash incident. The use of VR imagery to process the analysis results also has significant applications in test planning where geometric compatibility issues (e.g., potential contacts involving dummies and cabin-interior hardware with critical sensors and cameras) can be verified—prior to any testing. VR imagery and other features contained in the first-generation version of NCVM more than satisfied expectations, providing the impetus for the additional code development work reported herein. This effort produced new functionalities incorporated exclusively for this project.

The paper comprises seven additional major sections following this introduction. The first surveys pertinent literature that was reviewed and/or utilized. Sled testing and the application of strain gages to the surfaces of a hard plastic material commonly used for CRS shells are then highlighted, followed by a description of the MADYMO model employed in this research. Next is a detailed description of the current NCVM code as well as the upgrades made as part of this project. Model-forecasted strains and their experimentally measured counterparts are then compared and discussed and conclusions made regarding the model's predictive capability. The last section presents the overall conclusions derived from this study as well as several suggestions for possible future research.

LITERATURE REVIEW

Child Restraint System (CRS) design from both a usability and safety perspective has received considerable attention in both the U.S. and abroad. Presented below is a sampling of the published literature over the past two decades reflecting the research into methods for design, analysis, modeling and simulation. In the design area, such studies date back more than two

decades—e.g., an early examination of the factors that influence the selection and practical utility of CRS by Trinca and Arnberg [8]. More recent studies are exemplified by the harness design feature cost-benefit and harness usability assessment conducted by Rudin-Brown [9] and the use of numerical methods in CRS design by Lefeuve et al. [10]. The CRS misuse issue was first broached by Carlsson and Ysander [11]. As part of that research, they also advanced the safety-related advantages of using rearward-facing CRS for children up to four years of age. In another study on this subject, Arbogast et al. [12] compared serious injury and hospitalization incurred by two groups of similarly aged children: one restrained by forward-facing CRS, the other solely by seat belts. Subsequently, Czernakowski and Müller [13] quantitatively assessed the likelihood of potential misuse modes and estimated their effect on safety before and after corrective action.

Several studies have focused on modeling and simulation of CRS systems. Typical research comprising this category include a recent study by Noureddine et al. [14], which described the formulation of a reasonably accurate finite element model of the Hybrid III crash test dummy. In another more generic study by Arlt and Marach [15], an existing CAD tool was enhanced to develop a realistic three-dimensional child model suitable for CRS design and safety analysis purposes. Klinich et al. [16] utilized finite element modeling in conjunction with crash-reconstruction sled testing to investigate real-world infant head impact response and tolerance to skull fracture. Insofar as vehicular modeling per se is concerned, Thacker et al. [17] applied reverse-engineering methodology to an actual automobile to develop a corresponding finite element model suitable for use in crash-safety studies.

Finally, we note the studies dedicated to examining real-world crashes. The four-year CREST (Child Restraint System for Cars) project [18] investigated real-world crashes and conducted a number of full-scale crash reconstructions in an effort to gain a better understanding of CRS behavior and demonstrate that virtual testing can be an efficient design tool. Insights into the sources of data scatter always present in laboratory crash tests and its effect on (among other things) measured injury criteria was the focus of the recently developed ADVISER computer code [19]. The software automatically correlates numerical and experimental data and provides a corresponding quality rating for a numerical model. Of even more recent vintage is the Advanced Protective Systems (APROSYS) project [20], whose objective was to develop and introduce critical technologies that can improve passive safety for European motorists for relevant crashes of varying severity.

It should be noted that the CenTIR's initial CRS-related effort described in [6] integrated three separate design and crash-safety related focus areas: (1) sled testing, (2) digital computer modeling and finite element (FE) analysis, and (3) scientific visualization. Sled testing generated reliable, standardized empirical data and observations consistent with those delineated in FMVSS 213. Two different CRS use conditions were idealized by means of a MADYMO model that included a FE representation of the CRS shell, simulations conducted, and the results analyzed. Finally, a newly developed computer code utilized the three-dimensional simulation results obtained to create a virtual reality-type depiction of CRS and dummy response to the test conditions. To the best of our knowledge, none of the studies cited above or elsewhere have integrated all of these features.

The next section outlines the sled testing that constituted a vital part of this research.

SLED TESTING

The MADYMO model to be described later was "validated" in a series of sled test experiments performed at General Dynamics' HYGE sled facility. A current-production 5-point harness child restraint system (CRS) accommodating a Hybrid III 3-year-old child dummy was positioned upright on a modified FMVSS 213 test bench (described below) in the forward-facing installation mode. It was equipped with the standard array of electronic instrumentation: head- and upper torso-mounted triaxial accelerometer packages, upper neck force- and moment-measuring transducers, and a transducer that records chest compression.

Two series of three replicate tests involving two slightly different conditions were conducted with the same CRS—i.e., a total of six tests. The first series (test nos. 11-3-01, 11-3-02, and 11-3-03) utilized the manufacturer-supplied tether strap; the second set (test nos. 11-3-04, 11-3-05, and 11-3-06) did not. Figure 1 depicts two views of a typical pre-test setup.

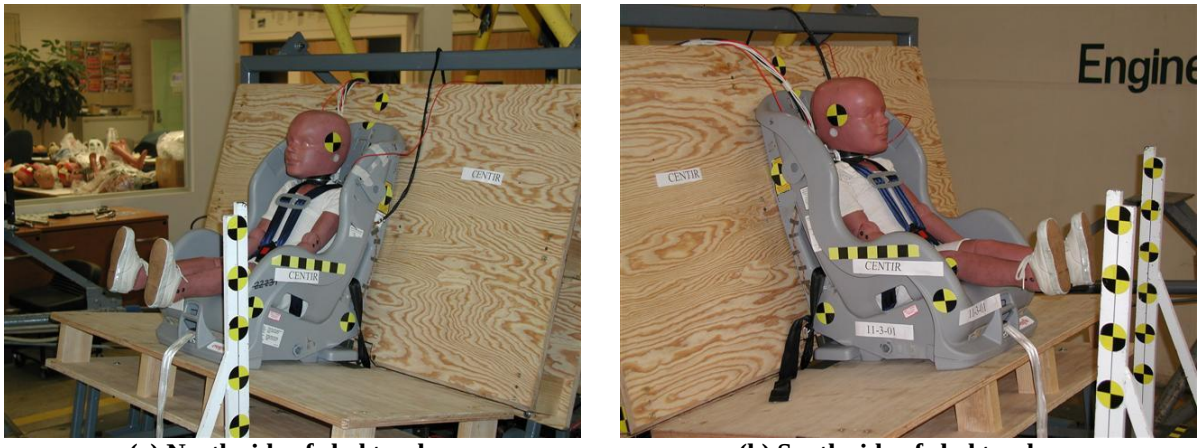

(a) North side of sled track **(b) South side of sled track**

Figure 1. CRS and dummy appearance immediately before a typical sled test.

Several changes were made to the FMVSS 213 test procedure in an effort to simplify the model and thus increase the possibility that its predictions would more closely match those obtained experimentally. The most notable of these was predicated on (1) the inherent complexity of the dynamic interaction between the CRS, dummy, and the bench upon which the base of the CRS rests; and (2) the absence of critical test bench material property inputs utilized by the MADYMO code. As such, the standard test bench, whose seat cushion and seat back assemblies are both "soft,"[4] was replaced by "hard" assemblies having the same overall exterior dimensions and geometry as their original counterparts. The latter units were constructed from ¾-inch-thick plywood and short lengths of nominal standard 2 x 4 (inch) lumber. Figure 2 shows the modified test bench bolted in place to the supporting steel framework.

[4] FMVSS 213 test bench cushions and backs are laminated constructs: two slabs of polyurethane foam having different density and thickness, the stiffer of which is in contact with a 3/8-inch-thick sheet of plywood. They are encased in a tight-fitting jacket made from elastic-backed vinyl automotive upholstery, circa early 1970s.

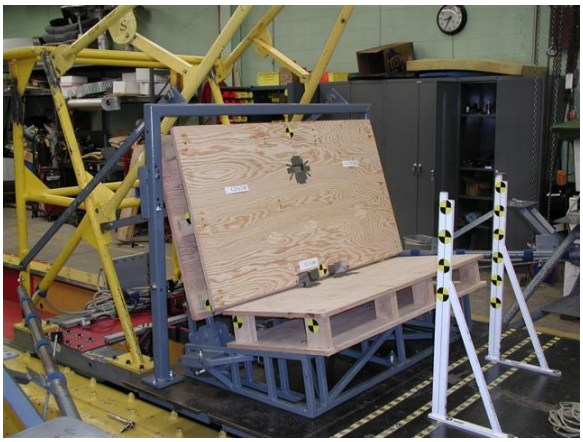

(a) Front view

(b) Rear view

Figure 2. "Hard" test bench.

In another attempt to improve the fidelity of the computer simulation, the seat back portion of the modified test bench was constrained against pitching action to eliminate possible inertial loading of the CRS during the tethered-configuration tests.[5] This objective was met by bolting two steel bars—one per side—between a vertical seat back frame member and the sled carriage structure (the arrow in Figure 2b points toward the south-side bar).

The CRS was secured to the sled carriage by a manufacturer-supplied seat belt assembly—commonly referred to as the "latch belt"—which passes through the appropriate belt path in the CRS shell. Each end snapped onto (via the hook provided) a belt anchor located below and behind the top plywood surface of the test bench seat "cushion." The free end of the webbing was then pulled through the buckle assembly until the belt could not be tightened any further. Figure 3 shows a typical pre-test latch belt installation. The above-noted anchors are shown in Figures 4a (the two arrows indicate their exact location relative to the longitudinal centerline of the test bench) and Figure 4b (a closeup side view).

Figure 3. Latch belt used to secure the CRS to the sled carriage.

[5] Conventional FMVSS 213 testing permits the seat back and its supporting framework to rotate about its pivot point.

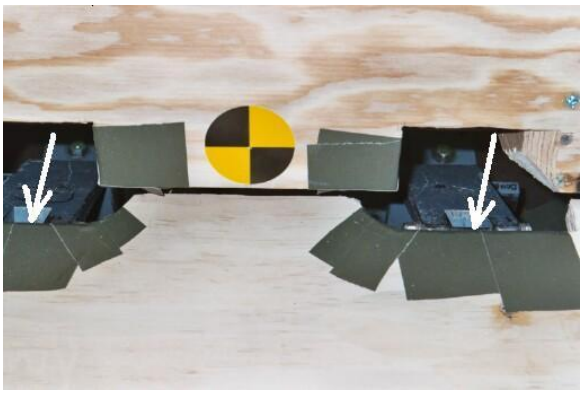

(a) Front view

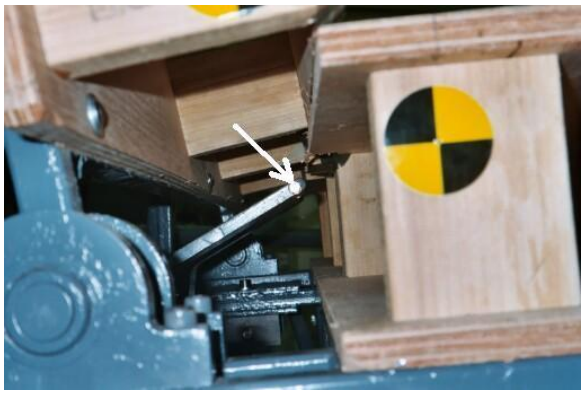

(b) Side view

Figure 4. Latch belt anchorage.

Other noteworthy departures from the FMVSS 213 test protocol included:

- Omitted the foam/fabric material that ordinarily covers the CRS shell.
- Installed load cells to record the tensile force variation in the upper torso harness straps and tether strap.
- Deployed three (instead of the customary two) high-speed video cameras:
  ─ a side-mounted narrow field-of-view camera to record CRS and dummy excursions consistent with the government test procedure.
  ─ a side-mounted wide field-of-view camera to capture the entire interaction between the CRS, dummy, and the back surface of the test bench during CRS/dummy rebound action.
  ─ a front-mounted camera along the longitudinal centerline of the sled carriage to record frontal-perspective CRS and dummy kinematics.

Five strain gage rosettes recorded strains at anticipated high-stress locations on the CRS shell. Details regarding these transducers and their application are presented in the next section.

Figure 5 is a front view of a typical pre-test setup. Both upper straps comprising the harness assembly were threaded through their respective top-level slots in the shell, with the above-noted load cells installed near dummy shoulder level. Prior to each test, the harness was hand tensioned as tight as possible and the chest clip adjusted to the same location.

Figure 5. CRS with dummy: front view.

Photos showing a typical tether strap configuration utilized in tests 11-3-01, 11-3-02, and 11-3-03 are presented in Figures 6 through 9. The arrow in Figure 6 points toward the origin of this belt—a thick double-slotted metal plate (designed to accommodate a loop in the fabric) lying flush against the rear shell wall. There the tether passed through a notch (indicated by the arrow in Figure 7) in the front-facing plywood panel of the test bench back assembly, emerged through an identical notch on the rear panel of this unit, and was clipped to an anchor mounted on the sled carriage framework (see Figure 8). The strap was hand tensioned to the maximum degree possible; the load cell (denoted by the arrow in Figure 9) spanned the gap between these two panels.

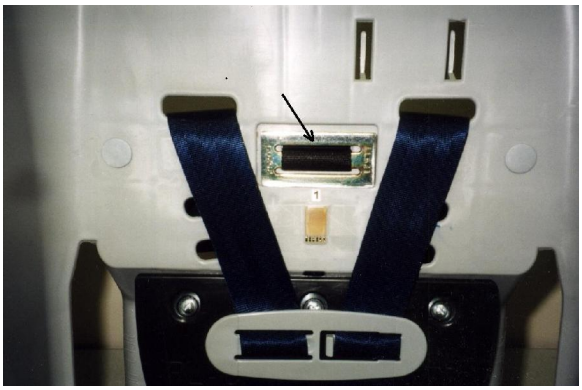

Figure 6. Tether strap mounting location on the CRS shell.

Figure 7. Test bench back assembly showing notch made to accommodate the tether strap.

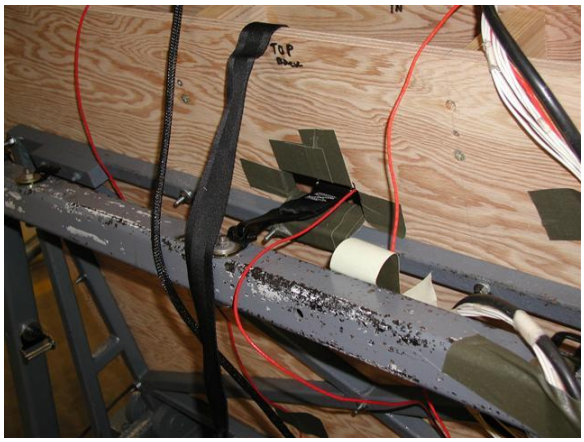

Figure 8. Tether strap anchorage behind the test bench.

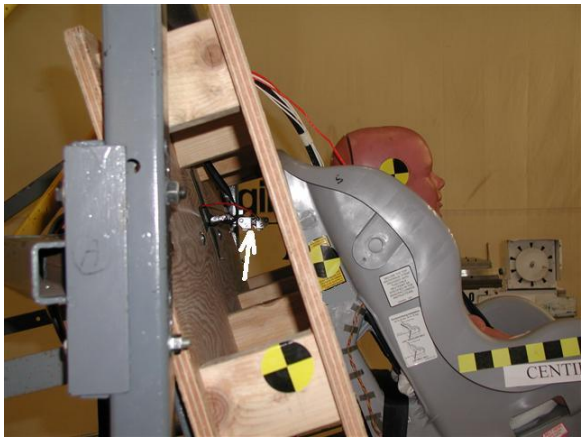

Figure 9. Tether strap load cell.

General Dynamics' Sled Facility generated virtually identical acceleration pulses for all six tests, each well within the corridor stipulated by FMVSS 213. A typical pulse, depicted in Figure 10, provided an average sled carriage velocity change of 29.7 mph.

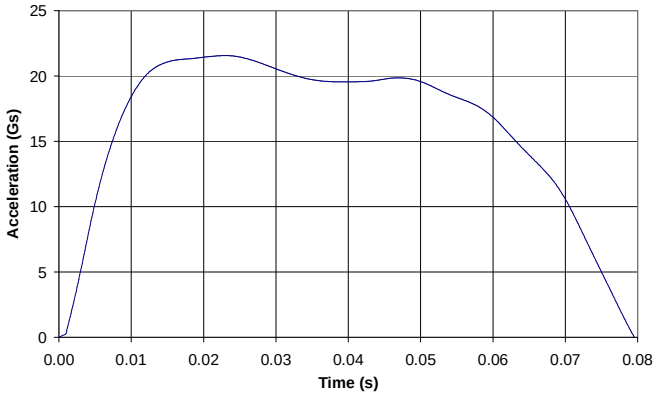

Figure 10. Typical FMVSS 213 sled acceleration pulse.

Figure 11 presents two photos showing the CRS and dummy following a typical sled event. The CRS sustained no visible damage during the first three (with tether strap) tests. Peak harness and tether belt forces were well below their respective maximum design limits, confirming the observed absence of any measureable permanent belt stretch after every test.

(a) North side **(b) South side**

Figure 11. CRS and dummy appearance immediately after a typical sled test.

The fourth test (no. 11-3-04)─the first without the tether strap─caused the first visually apparent damage to the CRS. Two small cracks formed in the upper portion of the shell (indicated by the arrows in Figure 12). The south-wide camera clearly revealed the crack-producing mechanism: head contact with the shell during rebound-induced CRS impact with the test bench back assembly. The photo shows that the cracks occurred in relatively narrow strips of plastic in an area containing several slots. As such, it was not regarded as a *structural* failure per se, and testing continued. Inspections following the two remaining exposures showed that neither one exacerbated the existing cracks nor caused additional shell damage elsewhere. Harness belt loadings were once again well within the elastic range for all three nontethered-condition tests.

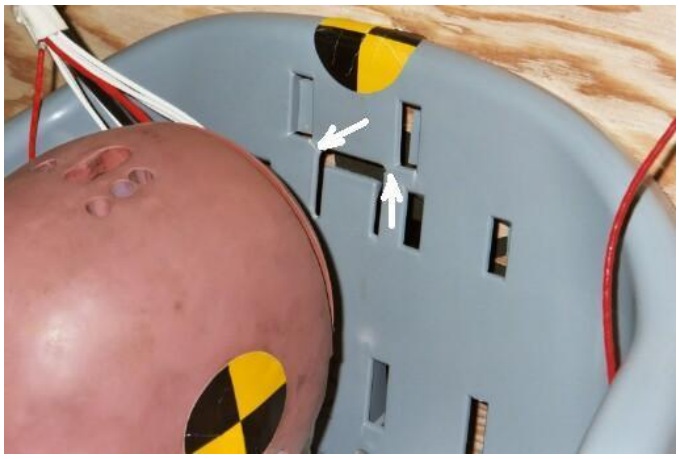

Figure 12. Small nonstructural cracks in the CRS shell detected after test 11-3-04.

The next section looks at the strain gage instrumentation employed as part of the test effort.

STRAIN GAGE MEASUREMENTS OF CRS SHELL DEFORMATION

Strain gage rosettes were affixed to the polypropylene (a plastic) shell of the CRS to measure empirical data that were converted (after appropriate processing) into principal strains. As will be discussed later, the latter information—if reasonably accurate—could be used to assess the fidelity of MADYMO-predicted principal strain (and hence stress) variation in a CRS shell during a dynamic test exposure.[6] This section presents some pertinent background information about strain per se that may be instructive for certain readers, followed by a brief narrative describing where and how the rosettes utilized in this research were installed.

The thickness of a typical CRS shell is roughly two orders of magnitude smaller than its other two characteristic curved- or flat-plane dimensions. Accordingly, load-induced deformations along its thickness can be neglected, permitting three-dimensional strain at any point on its surface to be approximated as a plane strain condition. Maximum and minimum normal strains—so-called principal strains[7]—can be calculated using the values of any three independent strain components measured at the same point by a rectangular strain gage rosette. Planar-construction general-purpose three-element 45-degree transducers (see Figure 13) were utilized in this effort. Gage specifications are provided in the Appendix.

Polypropylene is a somewhat "slippery" material, making gage-to-CRS bonding an especially challenging task—even for an experienced technician.[8] Technical assistance from the strain gage manufacturer along with extensive trial-and-error benchtop experimentation finally led to an installation procedure that provided satisfactory (non-slip) bond integrity between the two surfaces. That process is outlined in the Appendix.

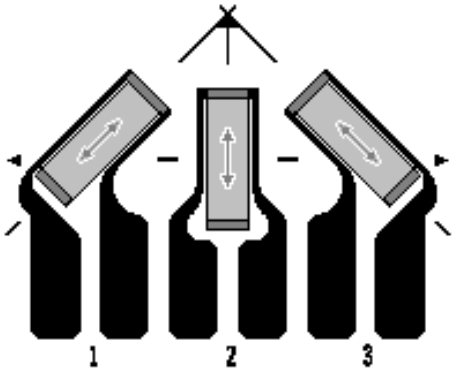

Figure 13. A typical planar-construction rectangular strain gage rosette.

[6] Except in some cases of contact stresses on the outside surface of a body, it is impossible to measure stress directly. Consequently strain is usually recorded, from which stress can be calculated.

[7] At any point in a biaxially stressed body (e.g., the CRS shell considered in this paper), there are two orthogonal planes on which shear strains do not exist. The normal strains on these planes are called principal strains—one a minimum magnitude, the other a maximum. Corresponding normal stresses are referred to as principal stresses.

[8] It is interesting to note that a comprehensive literature search subsequently conducted for this paper failed to uncover any published work that addressed strain gage installation on the surface of a CRS shell.

Five strain gage rosettes were installed on the shell at anticipated high-stress locations based on discussions with the CRS manufacturer and observations made during previous sled testing involving similar device designs. Gage nos. 1, 2, and 3 were cemented to the inside back surface of the shell, as shown in Figures 14 and 15. Gages were also installed on the outside shell surface just below the two belt passage slots (one of these, no. 5, is depicted in Figure 16)[9]

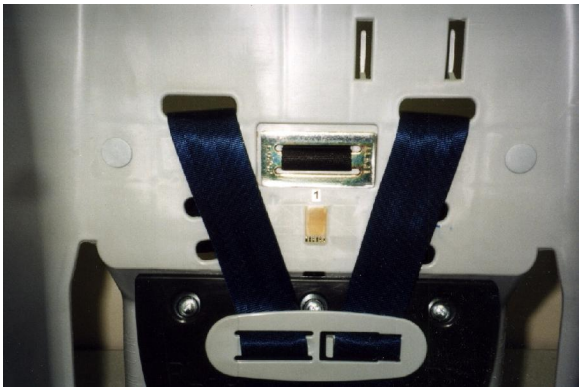

Figure 14. Strain gage rosette 1 was installed below the tether belt anchorage location.

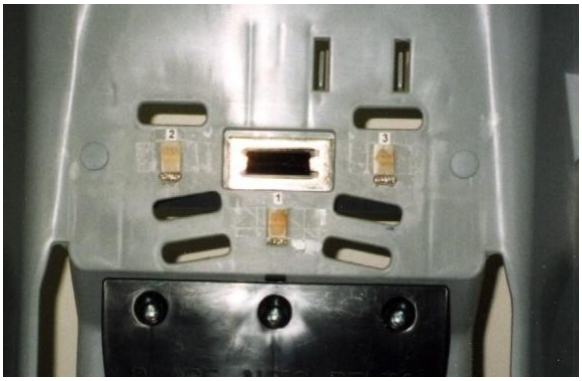

Figure 15. Stains were also measured at locations 2 and 3, beneath slots that permit harness strap passage.

As alluded to earlier, the strain-time data was processed to generate plots of maximum and minimum principal strains. Analyses of these curves, many of which are presented and discussed in the "RESULTS AND DISCUSSION" section, indicated that bond integrity was maintained for virtually the entire series of sled tests.

The next section describes the construction of a MADYMO computational model that provided a reasonable approximation to dummy kinematics and other pertinent parameters that govern crashworthy CRS design.

[9] Locations 4 and 5 are symmetrical with respect to the longitudinal-vertical plane that bisects the CRS shell .

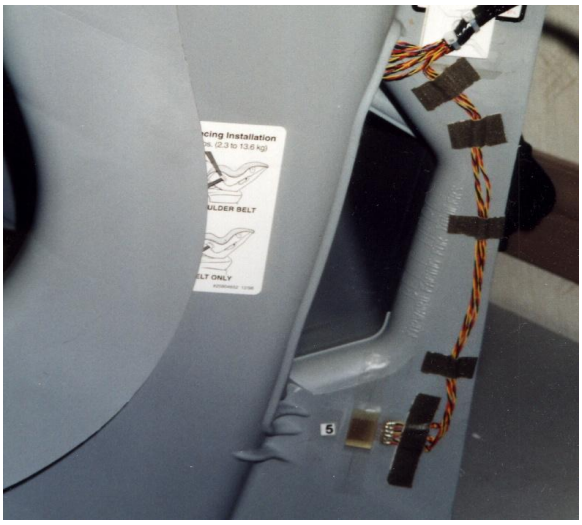

Figure 16. Rosette 5 was installed below a latch belt-shell contact region.

MODEL DEVELOPMENT AND TEST SIMULATION

The MADYMO model created for use in this study is intended to mimic the salient parts of the various systems and subsystems comprising the modified FMVSS 213 sled test setup described earlier. As such, it includes relatively simple idealized representations of the CRS shell and harness belt assembly, a standard Hybrid III 3-year-old dummy [21], the test bench assembly, and latch belt. Force-deflection characteristics and other material-related parameters utilized by MADYMO were generally unavailable, necessitating the use of assumed or best-estimate values gleaned from various sources.

As noted previously, CRS shell thickness is considerably less than its characteristic curved- or flat-plane dimensions. As such it was idealized using two-dimensional (shell-type) finite elements (FE) throughout.[10] HyperMesh v 5.0 [22] was used to generate a 17,150-element mesh that provided a reasonably accurate representation of the actual structure. This model replaced a coarse-mesh version (comprising only 2,850 elements) developed for use in the CenTIR's initial CRS research program [6]. The original and upgraded shell models are depicted in Figure 17.

The hard test bench described earlier was modeled as two rigid planes connected to inertial space. Individual belts comprising the harness assembly were all idealized as hybrid models consisting of a FE belt model connected to a conventional belt model [7] at each end.[11] The latter elements provide the mechanism to prescribe FE belt tension and are therefore instrumental in studying the effects of belt slack. Figure 18 depicts the MADYMO composite CRS/dummy model exercised in this study.

[10] These elements are computationally more efficient than their three-dimensional (solid) counterparts.

[11] MADYMO's conventional belt is a massless, uniaxial element that does not exhibit bending or torsional stiffness. In a systems context, it can be thought of as a spring connected in parallel to a damper. Spring and damper forces are calculated at the belt attachment points.

In an actual HYGE sled test, a prescribed x- or longitudinal-direction acceleration pulse (see, e.g., Figure 10) is applied directly to the sled carriage. The carriage and an attached simulated cabin or test fixture move backward, causing an initially at-rest occupant "connected" in some manner to one of those systems to *move forward relative to the cabin or fixture*. In MADYMO, a pulse can be applied directly to the dummy as a fictitious acceleration field and the calculated accelerations corrected to obtain the actual response. This option eliminates the need to model the sled carriage itself.

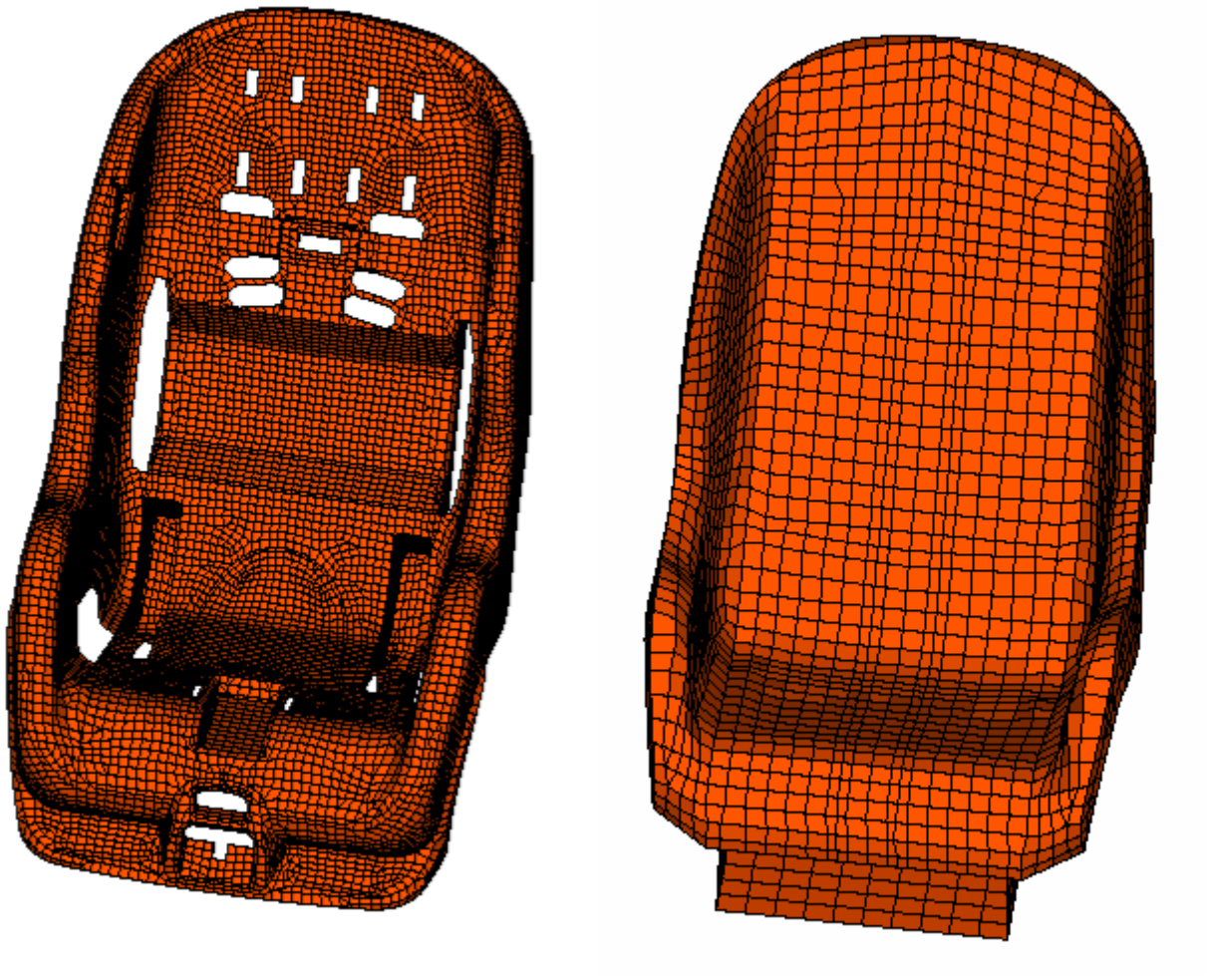

(a) **(b)**

Figure 17. Fine (a) and coarse (b) finite element CRS shell models.

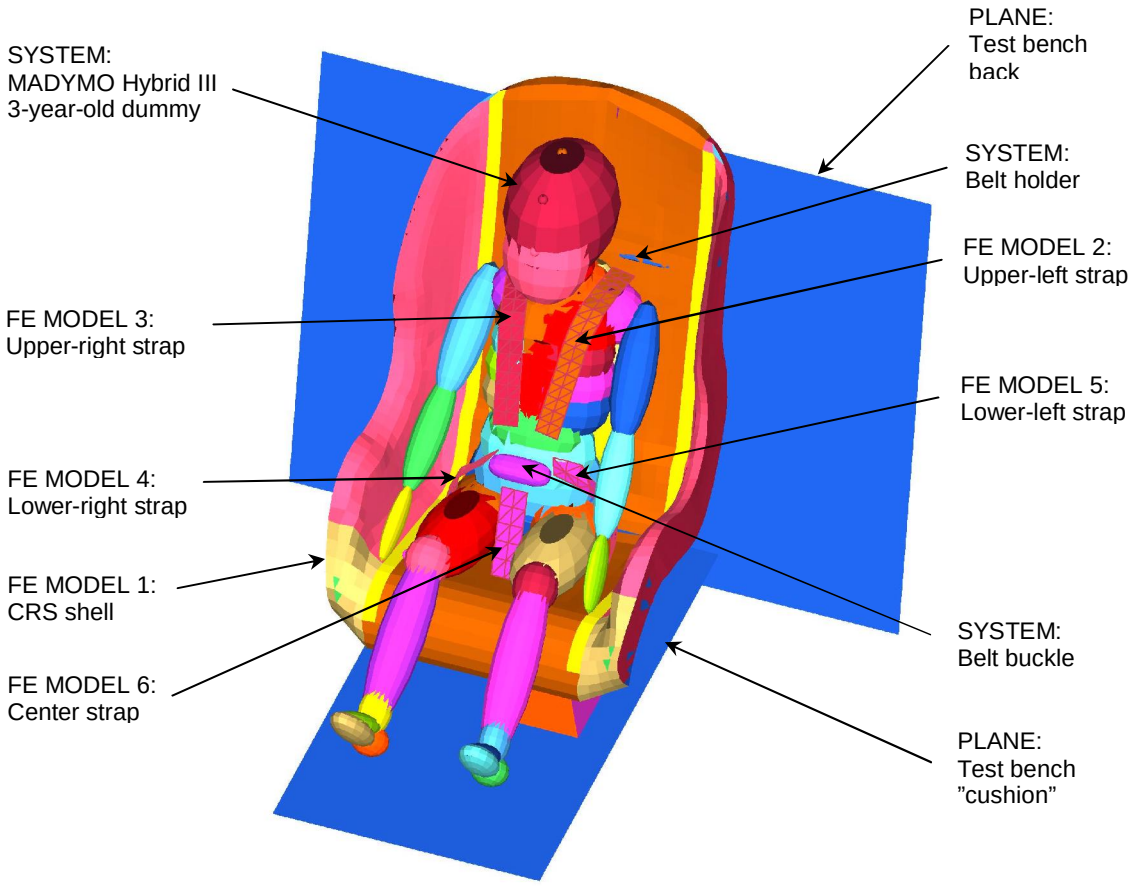

Figure 18. MADYMO composite CRS/dummy model.

The sled pulse and the (constant) gravity field were utilized as acceleration inputs to the model. A total simulation run time of 200 milliseconds (0.2 seconds) was prescribed, more than enough to observe the effects of CRS/dummy interaction with the test bench seat back during rebound.

Selected MADYMO-generated output from a model similar to the one depicted above is utilized in the next section to illustrate some of the capabilities afforded by the CenTIR's NCVM computer code.

THE NYSCEDII CRS VISUALIZATION MODULE (NCVM)

Traditional automotive design utilizes detailed *physical mockups* of the vehicle and its interior cabin configuration to study the design and evaluate human factors and ergonomic issues. Such prototypes are expensive, time consuming to develop, and difficult/impossible to modify once built. Scientific visualization (i.e., immersive virtual reality) provides an effective alternative. A suitable virtual prototype can replace a physical mockup to study design aspects such as product layout, component visibility, reachability and accessibility, clearances and collision detection, and design aesthetics [23].

Numerous recent studies have *qualitatively* discussed the merits of using scientific visualization for vehicle design and development purposes—e.g., to facilitate numerous design activities such as ergonomics, visibility assessment, and structural design. *Quantifying* the true utility of a virtual prototype, however, is often a problem. For example, one group of researchers noted that "one cannot provide a formal cost/benefit analysis at this time, since the technology has not yet been integrated fully into the daily productive work environment" of those who use these and other like technologies [24]. Numerous quasi-quantitative claims have been made that attempt to estimate the gained benefits of applied virtual prototyping. Indeed, a mid-1990's project determined that "up to 70% of the total life cycle costs of a product are committed by decisions made in the early stages of design" [25]. A virtual prototype that can be created in a relatively short period of time and is utilized properly can be instrumental in this regard, helping to significantly decrease product design-cycle time and cost [26].

The authors posit that scientific visualization can be successfully integrated into the crash-safety design of vehicular child restraint systems (CRS) via our recently developed utility, the aforementioned NYSCEDII CRS Visualization Module (NCVM). The first part of this section briefly outlines the design, development, and operability of the "first-generation" NCVM, which was applied to a MADYMO-based CRS/dummy model in a virtual crash environment [6]. It concludes with a description of several new functionalities that were incorporated into that code as part of the research described in this paper.

GEOMETRIC REPRESENTATION

NCVM incorporates information from a TNO-MADYMO simulation into a single, all-encompassing scientific visualization written in OpenGL [27], allowing it to be used on multiple platforms, including PC and SGI/Sun workstations. NCVM's fully integrated functionality provides a new mechanism by which scientists and engineers can make CRS-related design decisions more quickly and easily.

The baseline NCVM initializes by parsing and preprocessing pertinent TNO-MADYMO output files—geometry (.kn3), stress (.fai), and acceleration (.lac)—over a prescribed sled test simulation time interval. Standard OpenGL primitives are utilized to generate the geometry from the MADYMO .kn3 file at each time step. As noted in the previous section, the CRS shell and associated restraint belts were idealized in MADYMO as finite element models. Collectively these models comprise *thousands* of nodes, necessitating the use of solid primitives having the fewest number of vertices. Cube primitives, which have eight corner vertices, were employed in this research.

MADYMO representations of the test bench and latch belt were modeled as two simple planar quadrilaterals and line segments, respectively. That code's use of *hyperellipsoids* to model dummy geometry required creation of a new OpenGL primitive class: the *gluEllipse* (a modified version of the existing OpenGL "gluSphere" routine). Baseline and enhanced .kn3 CRS geometries are shown in Figures 19 and 20, respectively. The latter figure depicts both the CRS and a generic vehicle (shown partially transparent), including a back seat for the CRS, in the background—an attempt to enhance realism and add context to the graphics provided by the sled test simulation.

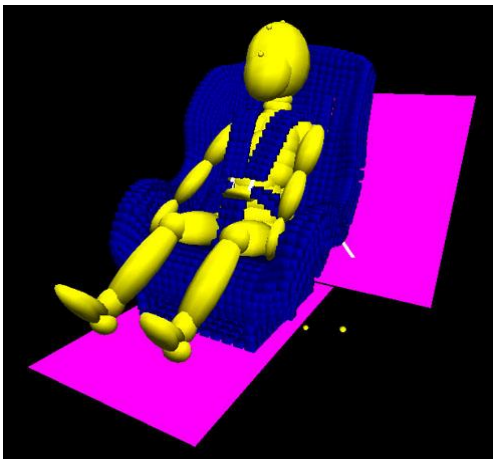

Figure 19. Baseline CRS geometry.

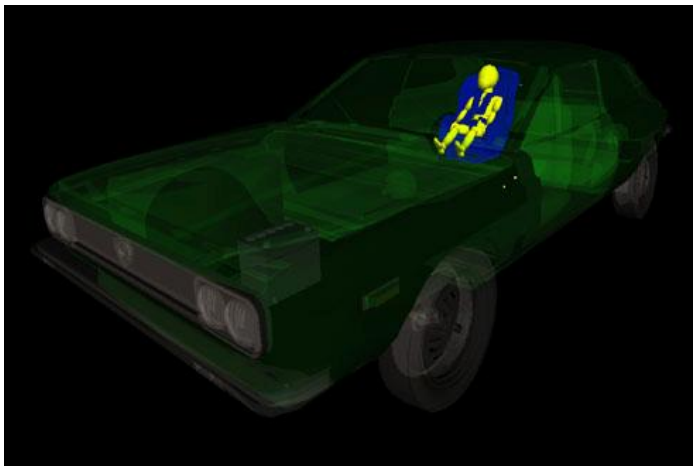

Figure 20. Enhanced CRS geometry.

SCIENTIFIC VISUALIZATION: FINITE ELEMENT AND ACCELERATION DATA

NCVM is more than just an animation depicting the displacement-time history of geometric models (here, the CRS and dummy) at every step of a simulation. It also incorporates useful technical information─notably, stress and acceleration─coincident with that motion, making it a truly *scientific* visualization. In the first case, MADYMO's .fai files provide the von Mises stress variation over time at the location of each geometric node in a finite element model. NCVM employs color-coded values of these stresses at every time step for each node to generate animated renderings of model stress contours. NCVM also provides an on-screen textual description of max/min/mean stress at each time interval.

Stresses can be monitored in three different modes: absolute (overall max/min stress over the entire simulation), logarithmic (which uses a natural log scale to compress the stress range to a smaller numerical region), or dynamic (absolute max/min stress as a function of time step). Figure 21 depicts a screen capture with relevant finite element contour information shown; here, overall stress in the finite element models is depicted in the "absolute" contouring scheme.

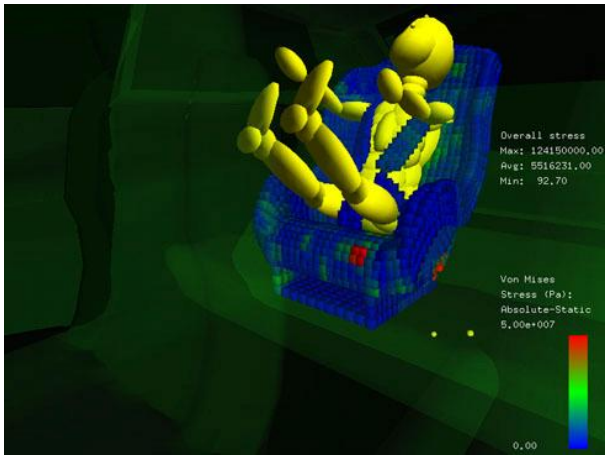

Figure 21. NCVM contour plotting feature.

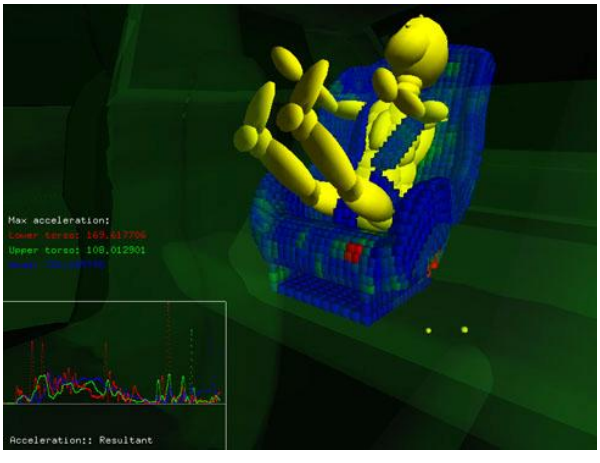

Figure 22. NCVM acceleration plotting feature.

NCVM can track the linear acceleration response (x, y, z, and resultant) of the dummy lower torso, upper torso, and head at every time step of the simulation by means of an on-screen plotting utility; color-coding distinguishes one parameter from another. A textual description of max/min/mean acceleration with time step is also provided. The default plotting mechanism shows the graph interactively together with test-induced motion in the lower-left portion of the screen. Should the user wish to see more intricate plotting details, a "full-screen" plotting mode is available to more precisely observe the acceleration profiles at each time point. Figure 22 depicts an example screen capture of resultant acceleration curves and a listing of their respective maximum values.

NCVM: EXPANDED OPERABILITY

Since its preliminary development, numerous features have been added to the NCVM to enhance its potential usability to the CRS research community. Three such features recently incorporated into the NCVM are described and demonstrated below.

Dummy vapor trails

The baseline version of the NCVM allows the user to track geometric changes of the dummy and CRS during their respective motions by visualizing frame-by-frame changes in global position of these elements (in this example, over a 0.2-second, 67-frame simulation). The authors theorized that it might be useful to have some means of visualizing the overall change in displacement all within a single frame. A newly incorporated "vapor trails" option which can be toggled on/off at any time provides this capability. It is illustrated in Figure 23.

As was the case with the semi-transparent vehicle, the above visual effect is accomplished by utilizing *alpha* values within OpenGL. For each vertex that comprises each ellipsoid of the dummy geometry, the user specifis an RGB color (3 parameters), and a fourth parameter called an alpha value─a measure of opacity. (Our dummy model used an R, G, B triplet of 1,1,0. Alpha was prescribed as 1.0 for the current frame, while nearly transparent "ghosted" values of 0.05 were employed for all previous frames.) In Figure 23 only the dummy form is vapor trailed; the same methodology, however, could be applied to each of the other CRS geometries, or all geometries simultaneously, if desired.

The authors plan to extend the vapor trail feature by allowing the NCVM user to simultaneously track and/or plot the trajectory of a user-selected location on the model. For example, the user might wish to simultaneously visualize both the vapor trail motion and a corner-screen plot (with tracked numerical values) of a spherical marker on the dummy's head. The left and right images of Figure 23, respectively, show these markers in their initial state as well as displaced and "morphed" later on in the simulation.

.

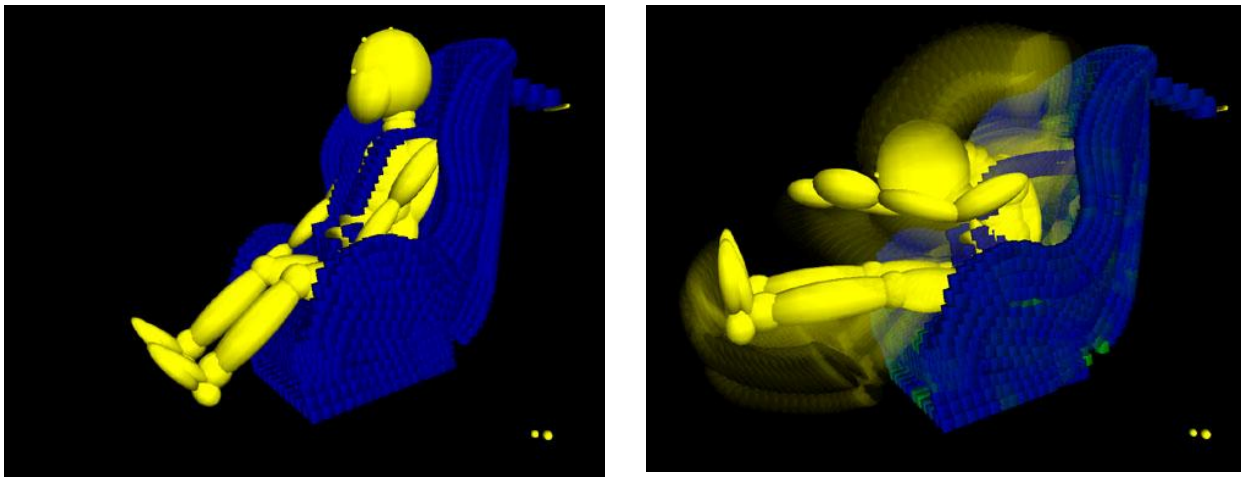

Figure 23. NCVM dummy "vapor trails" display option.

Menu-driven hot views

Presently, NCVM allows the user to fully navigate (i.e., translate/rotate/zoom) about the CRS/dummy models via the mouse and keyboard. The authors conjecture that a typical user may wish to quickly achieve one of numerous standard model vantage points. Useful possibilities include six orthogonal views (front/back, top/bottom, and left/right) as well as perhaps a conventional, default isometric front view. Accordingly, NCVM provides a simple "hot views" menu option. Figure 24 is an example showing the six currently available orthogonal perspectives.

The "hot views" feature will also have longer-term applicability for the NCVM and its relationship to the sled testing and modeling/analysis aspects of this research. Ultimately, the end goal of our research team is to devise a digital model that provides near-direct correlation with corresponding displacement-time responses documented in an actual sled test. Numerous high-speed videos showing CRS/dummy kinematics during FMVSS 213 and other sled test exposures are available; many of them include footage taken from vantage points similar or identical to those mentioned above. As such they would constitute the comprehensive empirical database needed for an envisioned real-time validation of the NCVM.

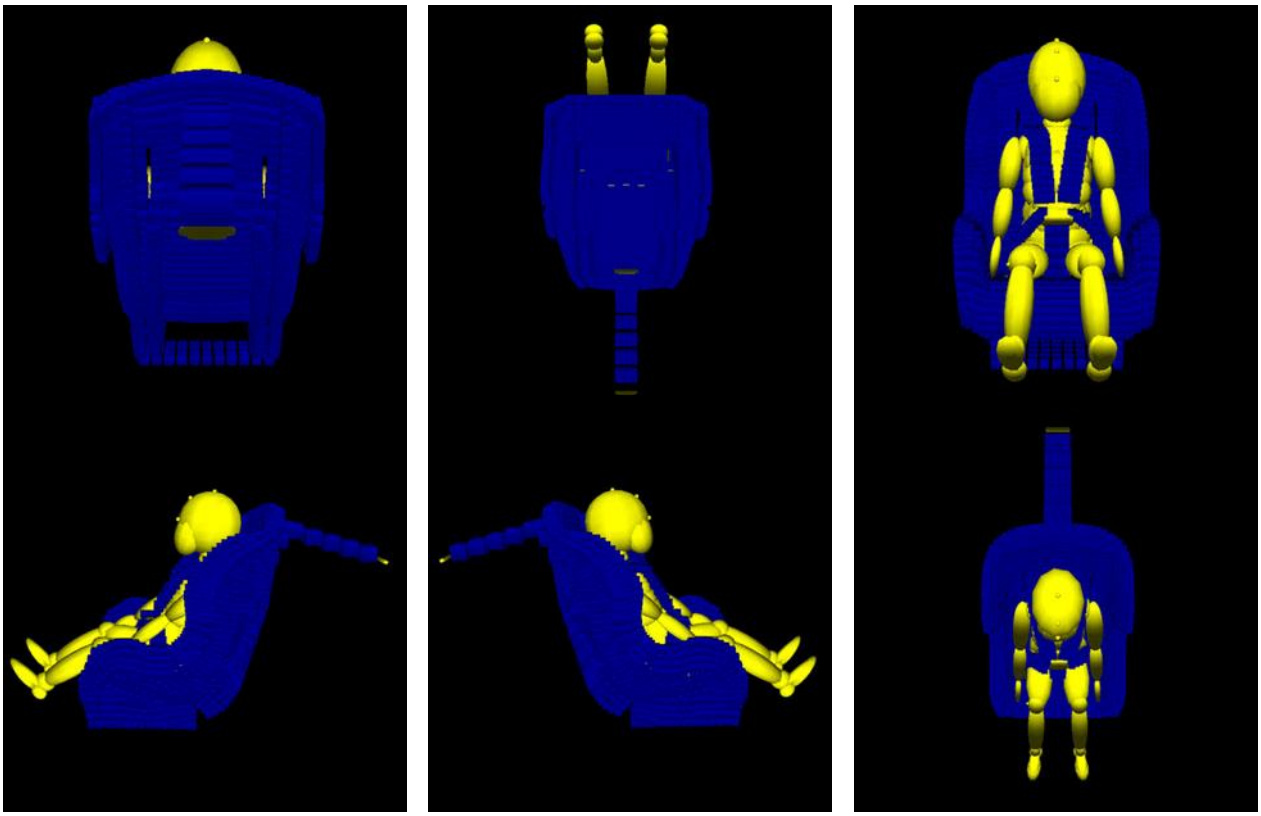

Figure 24. Six orthogonal NCVM-generated "hot views."

Volumetric slicing feature

In certain instances a user may wish to "slice" through a portion of the model geometry to attain a new (and more useful) perspective on whatever is being visualized. Such a feature would, for example, allow the user to (1) see "through" the CRS/dummy geometry to visualize a detail that might otherwise be hidden or obstructed by one of the other model constituents, and (2) observe possible collisions and/or interference between one or more such moving objects. It would be particularly beneficial as part of the aforementioned "enhanced" geometric arrangement, where the vehicle model encompasses the CRS/dummy configuration. Judicious slicing would enable the user to see inside the vehicle to observe certain critical portions of the CRS and/or dummy model geometries while still viewing those systems within the context of an actual vehicular crash scenario.

Volumetric slicing is accomplished through the use of *clipping planes* within OpenGL. Conventional screen clip coordinates dictate the viewing volume that is seen by the user on a two-dimensional computer screen: near, far, top, bottom, left, and right extents. OpenGL allows the user to specify up to six additional clipping planes defined in accordance with a standard plane equation. For preliminary purposes in the NCVM code, three additional clip planes have been defined that correspond to the three orthogonal global axes (i.e., $x = 1$, $y = 1$, $z = 1$). A simple translation command permits the user to utilize the keyboard to translate each of these clipping planes along a coordinate axis to "sweep" the clip plane over the geometry. This either exposes or hides the CRS geometry interactively for a given frame of the simulation. Figure 25

illustrates this feature. In the two upper images, the complete model geometry is shown from both a side and a top view, respectively. The two lower images are their respective counterparts; they depict the same geometry partially clipped along the y-axis of the CRS. Note that the clipped views allow us to still see the CRS in context; however, exterior geometries have been eliminated, providing a less obstructed view of both the CRS and dummy.

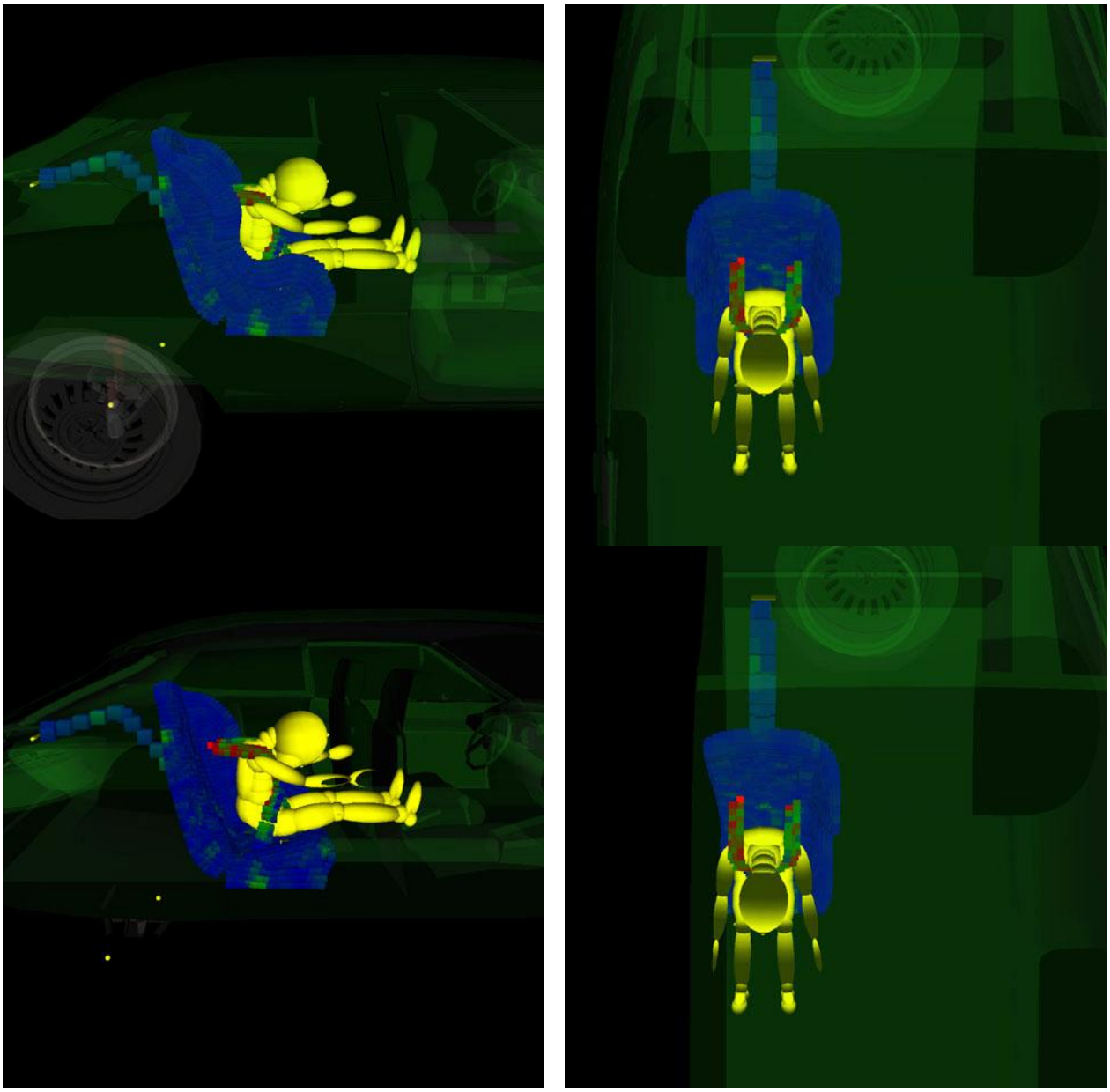

Figure 25. NCVM-generated "sliced" views using orthogonal clip planes.

The next section will present and discuss some of the experimental and analytical results that were generated in this project.

RESULTS AND DISCUSSION

This section compares corresponding computer-generated and experimental (i.e., sled test) results in order to ascertain the reliability of the MADYMO composite model. Model validation followed an evolutionary path. The first such evaluation was performed during the CenTIR's initial CRS-related research effort [6], with dummy body segment displacement and acceleration responses measured in sled testing serving as the "definitive" criteria against which model fidelity was evaluated (this assessment was deemed a highly subjective "good," considering the complexity of the real-world conditions being simulated). Upgrades made to that model as part of the current project provided better correlation. Figure 26, which compares predicted and test 11-3-04, 11-3-05, and 11-3-06 dummy upper torso accelerations, depicts one notable example.

Model validation was next extended to the structural realm by examining strain, a parameter of paramount importance in CRS crashworthy shell design. Strain gage data recorded in the sled tests were processed to generate principal strain-time plots that were compared to their MADYMO equivalents. As expected, the fine-mesh model illustrated earlier (see Figure 17a) provided significantly better correlation than the coarse-mesh version. This fact is readily apparent in Figure 27, which depicts the time variation of maximum principal strain measured at gage location 3 in tests 11-3-04, 11-3-05, and 11-3-06 relative to forecasted responses from both models. The ensuing discussions will accordingly be confined to the fine-mesh model.

Figures 28 through 32 compare model-generated strain estimates with corresponding processed experimental data obtained from the above three tests at each of the five instrumented locations. The predicted strain at location 1 displayed reasonably good agreement with respect to both the magnitude and timing of its initial peak.[12] Although this temporal estimate was also satisfactory at the other four locations, corresponding predicted initial peak accelerations were considerably lower compared to the experimental data. This disparity most likely reflects the use of numerous approximations in the MADYMO model. Most notable are (1) shell material property inputs obtained via quasi-static tensile testing instead of more suitable dynamic testing (thus ignoring strain-rate effects), and (2) the position and angle of the CRS on the test bench, which cannot be accurately modeled. Both sources can significantly affect model-predicted strain reliability.

Experimental peak strain magnitudes obtained from tests 11-3-04, 11-3-05, and 11-3-06 exhibited a considerable spread at every gage location. Much of this disparity probably stems from always-present differences in dummy positioning relative to the CRS shell as well as similarly expected variations involving harness positioning and tension. The inherent sensitive nature of strain gauges per se may also have been a contributing factor.

It's interesting to note that gauge rosettes 2 and 3 as well as 4 and 5 are respectively symmetrical with respect to the CRS longitudinal-vertical plane. MADYMO-predicted strains at these locations were (as expected, by default) virtually identical, but their experimental counterparts displayed notable differences in magnitude and timing. Such variance is not uncommon—another one of the many vagaries associated with dynamic-type experimental testing.

[12] Strains recorded after about 0.14 seconds reflect the effects of CRS contact with the test bench seat back during that device's rearward motion. This impact is very unpredictable in the experiment and cannot be simulated with any appreciable degree of confidence by the model. All discussions therefore will consider only the *initial* peak strain.

Figure 33 compares the tensile force profiles obtained from test 11-3-05 left and right harness straps to the corresponding curves predicted by the model. The latter force levels were significantly lower than those measured experimentally—probably because of the estimated belt material property inputs (as well as other approximations) utilized in the model.

"What-if" analyses were conducted with the validated model to ascertain the optimum locations to measure—as part of a hypothetical series of sled tests—CRS shell strain for use in (1) model validation activities, and (2) material failure analyses. A single MADYMO material parameter input (Young's modulus for polypropylene) was varied at different points on the shell. Three simulations were conducted and the sensitivity of model-predicted strains observed. One run used an experimentally determined (via tensile testing of the actual shell material) value. The other two simulations were conducted with moduli that deviated +/-25% from the latter baseline.

Figure 34 shows how the above perturbations affect the *peak value* of maximum principal strain at the 11 locations considered (see Figure 35). Figure 36 compares predicted peak strain using the baseline and perturbed Young's modulus inputs to that recorded at three different *actual* transducer installations in sled tests 11-3-04, 11-3-05, and 11-3-06. Strain variation at a point *on the model* near the (artificial) lower-right harness anchorage location—see point 5 in Figure 35—is shown in Figure 37. Based on the results obtained, locations 5, 6, 7, and 9 are the most sensitive to material property changes and incur the highest strain; strains at locations 1, 2, and 3 exhibit much smaller sensitivity. Because of material property uncertainties, locations 1, 2, and 3 would probably provide data most suitable for test validation purposes. Conversely, failure analyses should use worst-case data from locations 5, 6, 7, and 9.

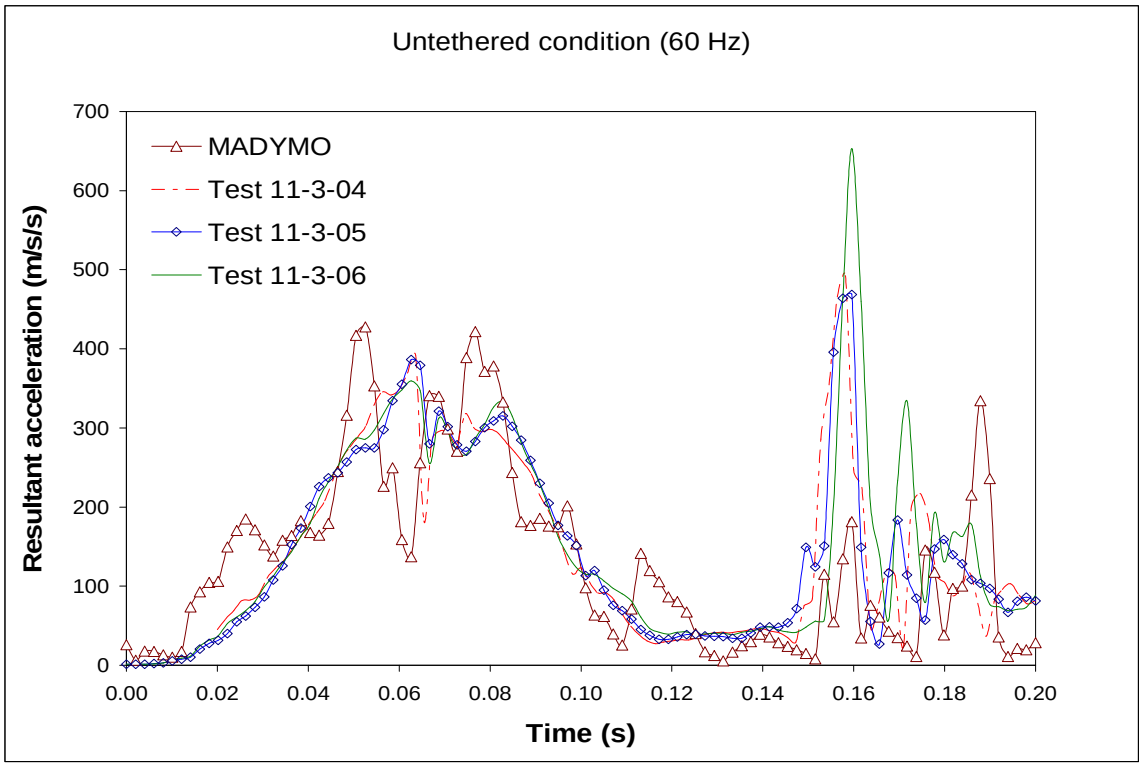

Figure 26. Resultant upper torso acceleration from MADYMO model and three replicate sled tests.

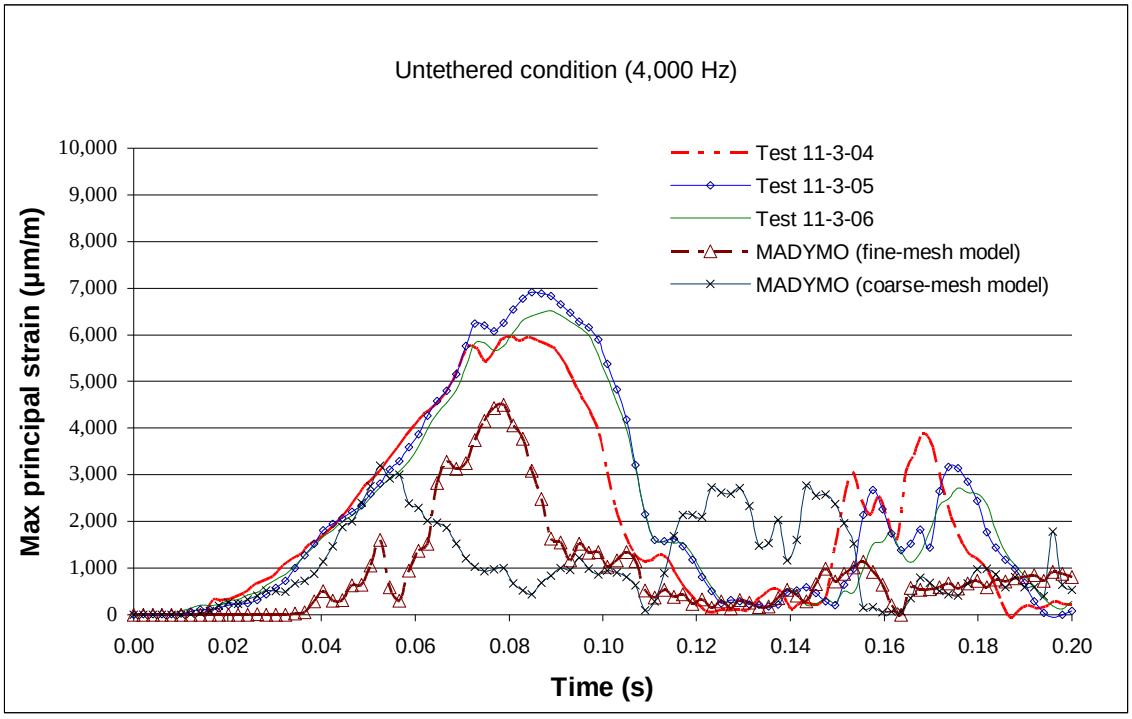

Figure 27. Location 3 strain: test results and MADYMO coarse- and fine-mesh model predictions.

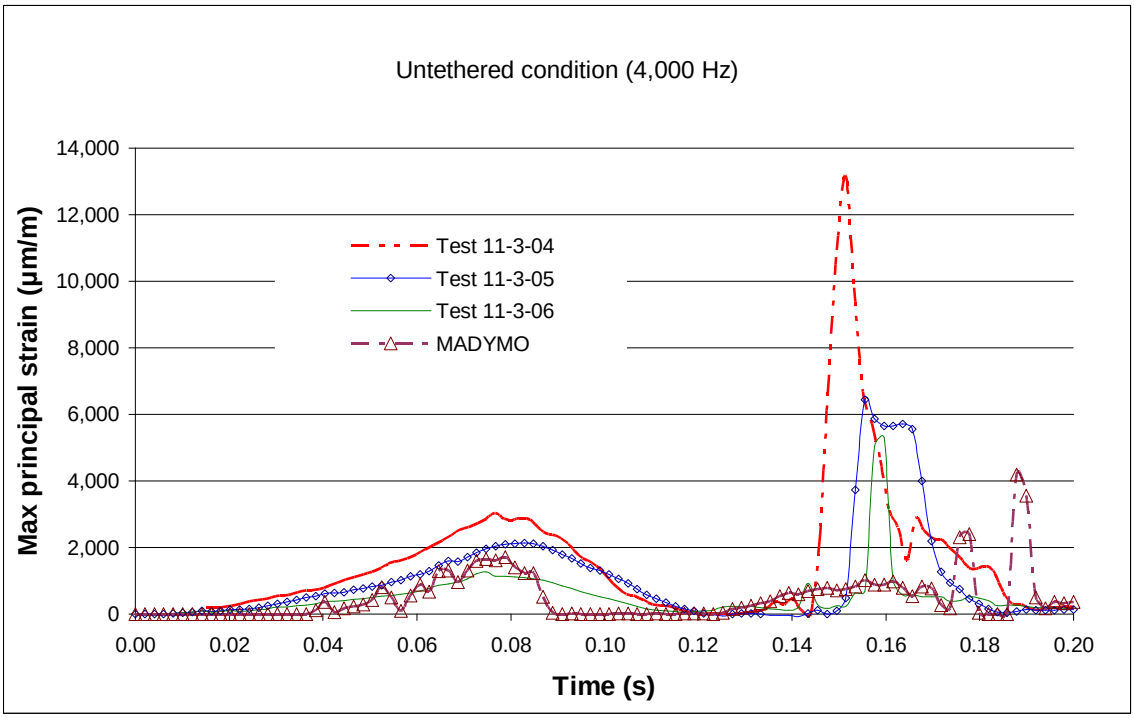

Figure 28. MADYMO-predicted and measured strain at rosette location 1.

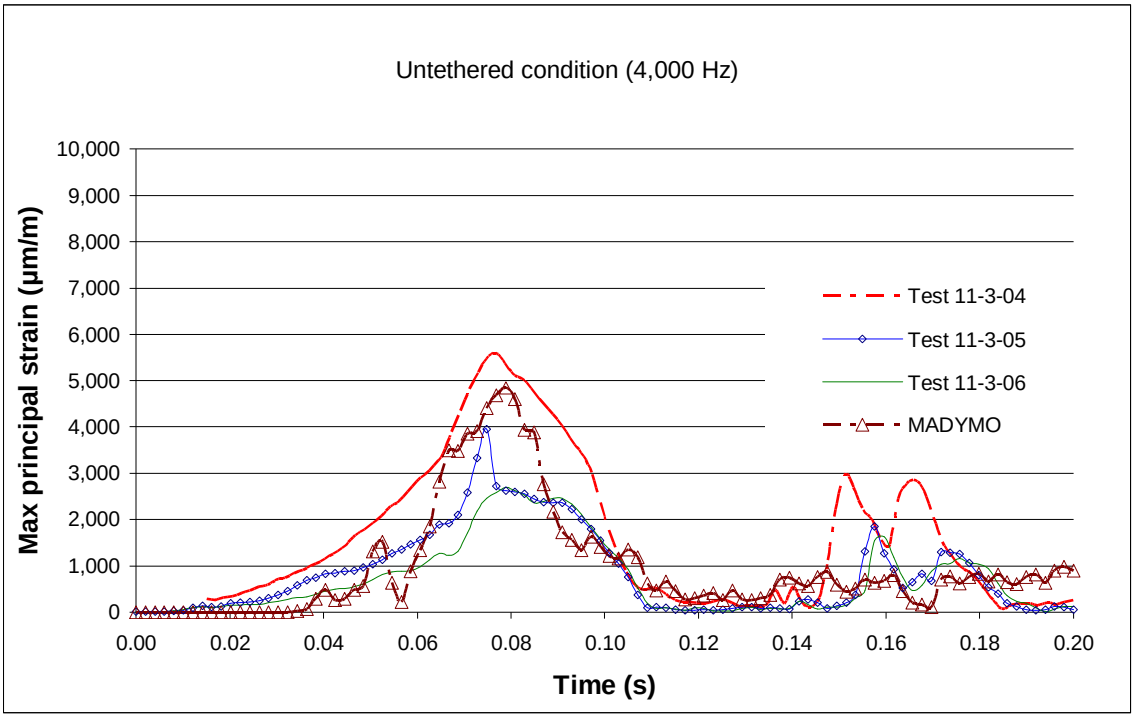

Figure 29. MADYMO-predicted and measured strain at rosette location 2.

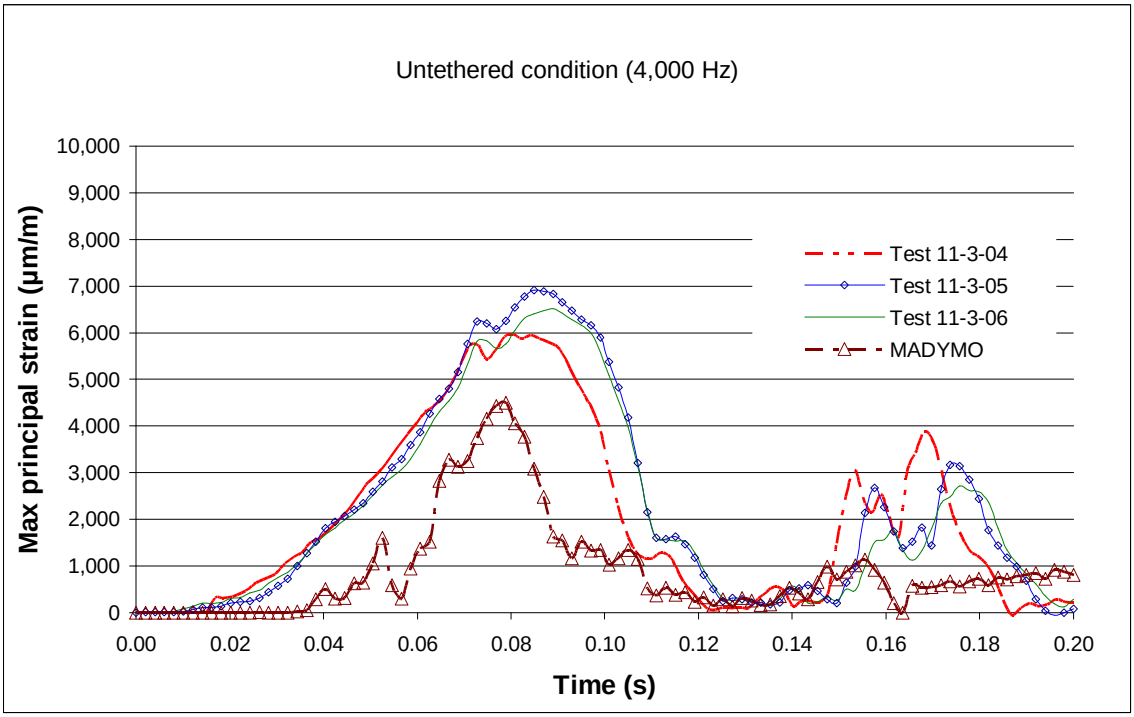

Figure 30. MADYMO-predicted and measured strain at rosette location 3.

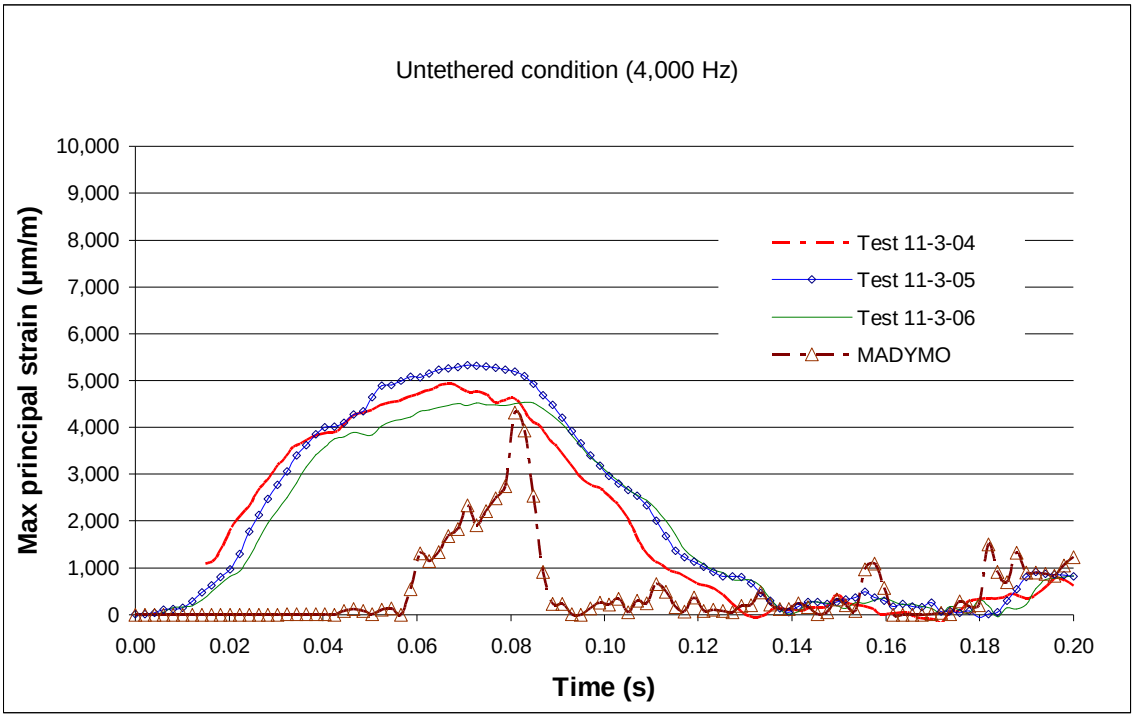

Figure 31. MADYMO-predicted and measured strain at rosette location 4.

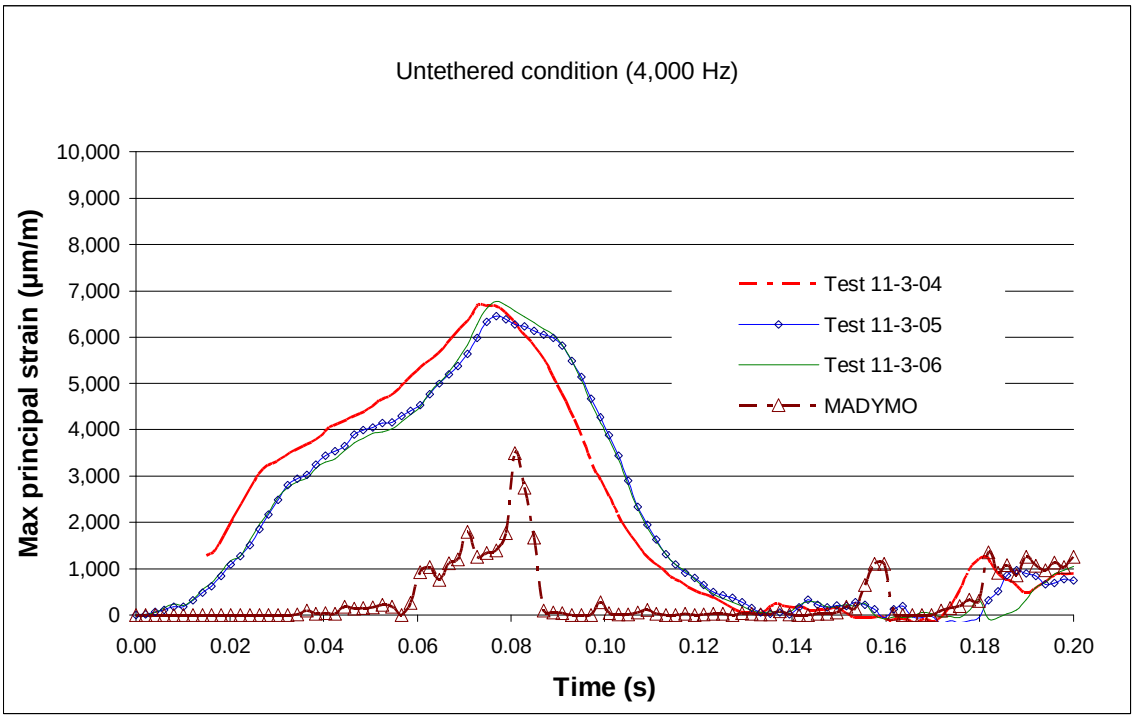

Figure 32. MADYMO-predicted and measured strain at rosette location 5.

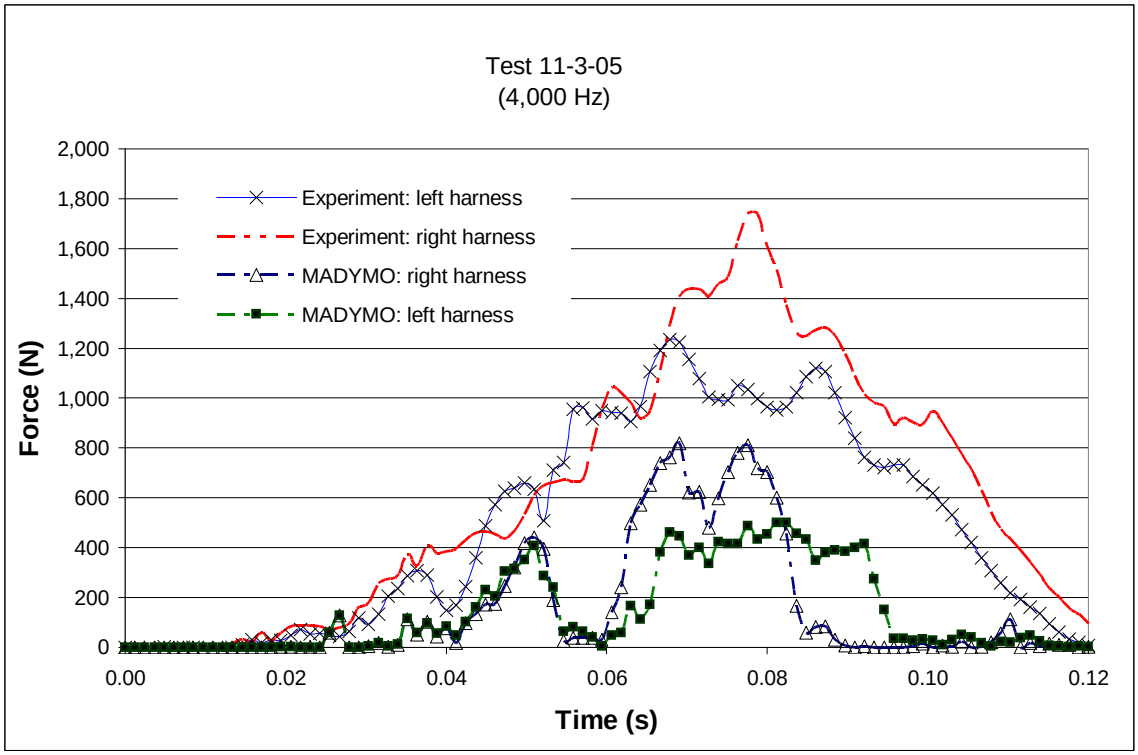

Figure 33. Harness strap forces: MADYMO-predicted and measured in test 11-3-05.

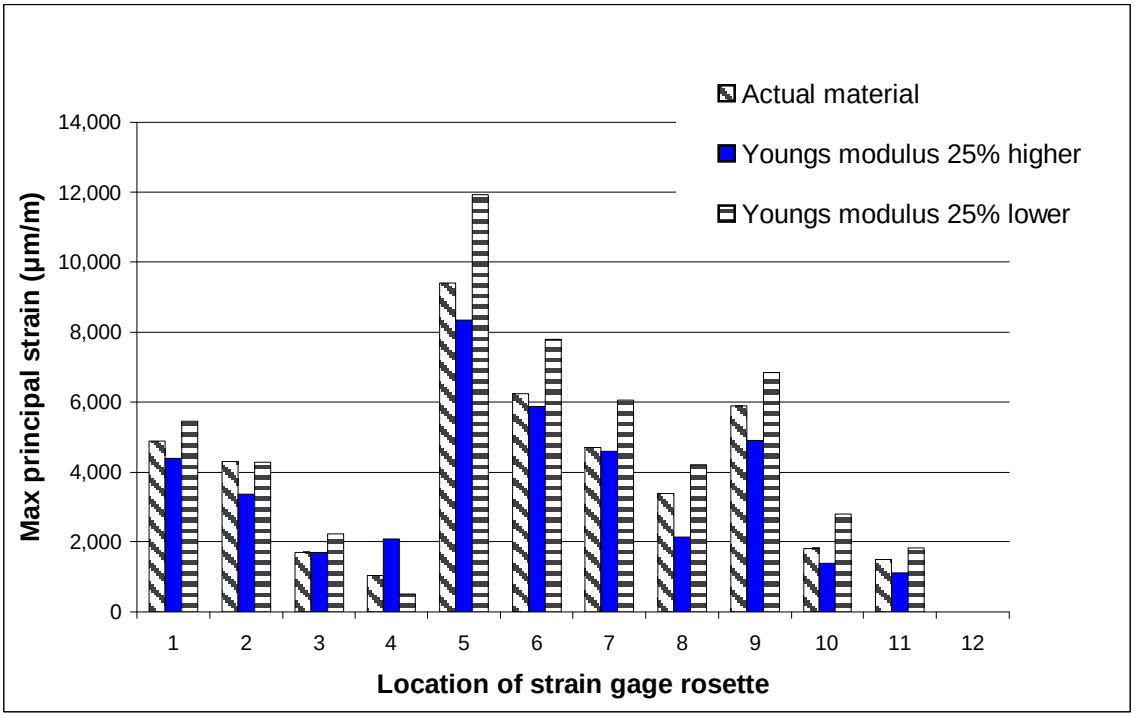

Figure 34. Sensitivity of maximum principal strain with transducer location.

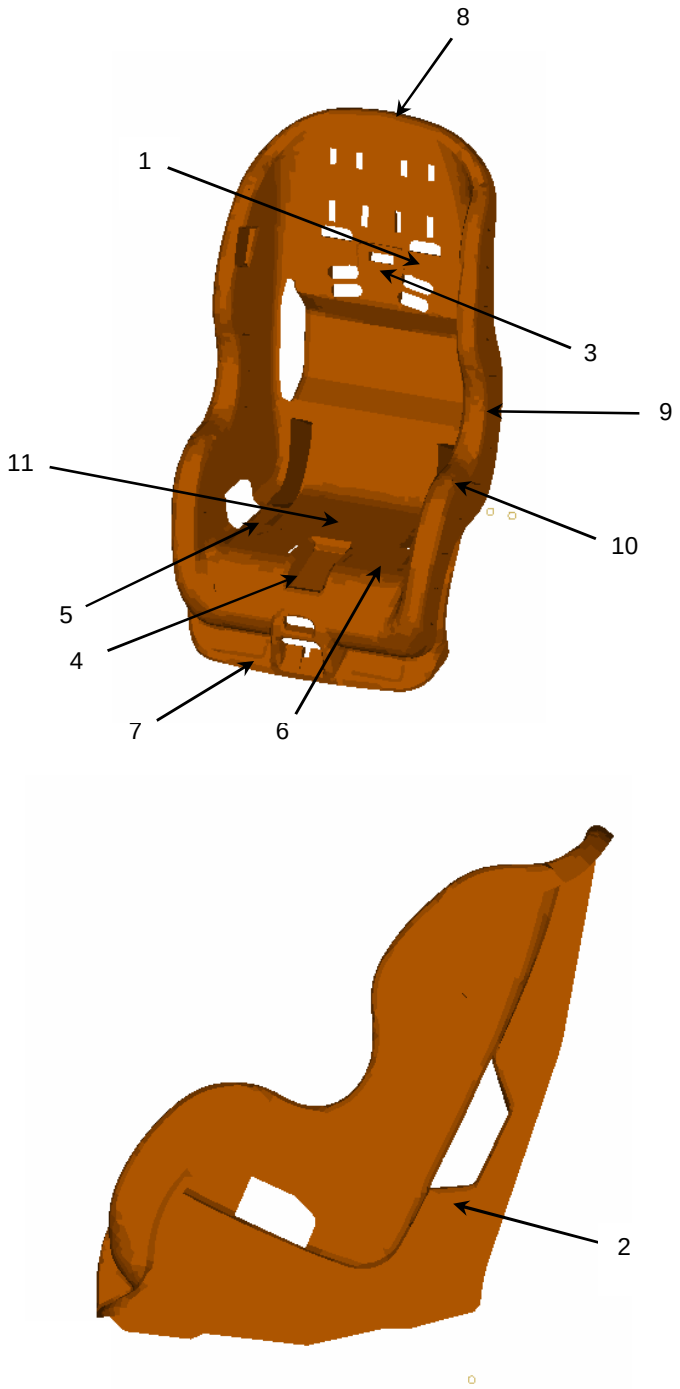

Note: The above gage locations differ from those used in the sled test experiments.

Figure 35. Strain gage rosette locations specified for use in the model perturbation study.

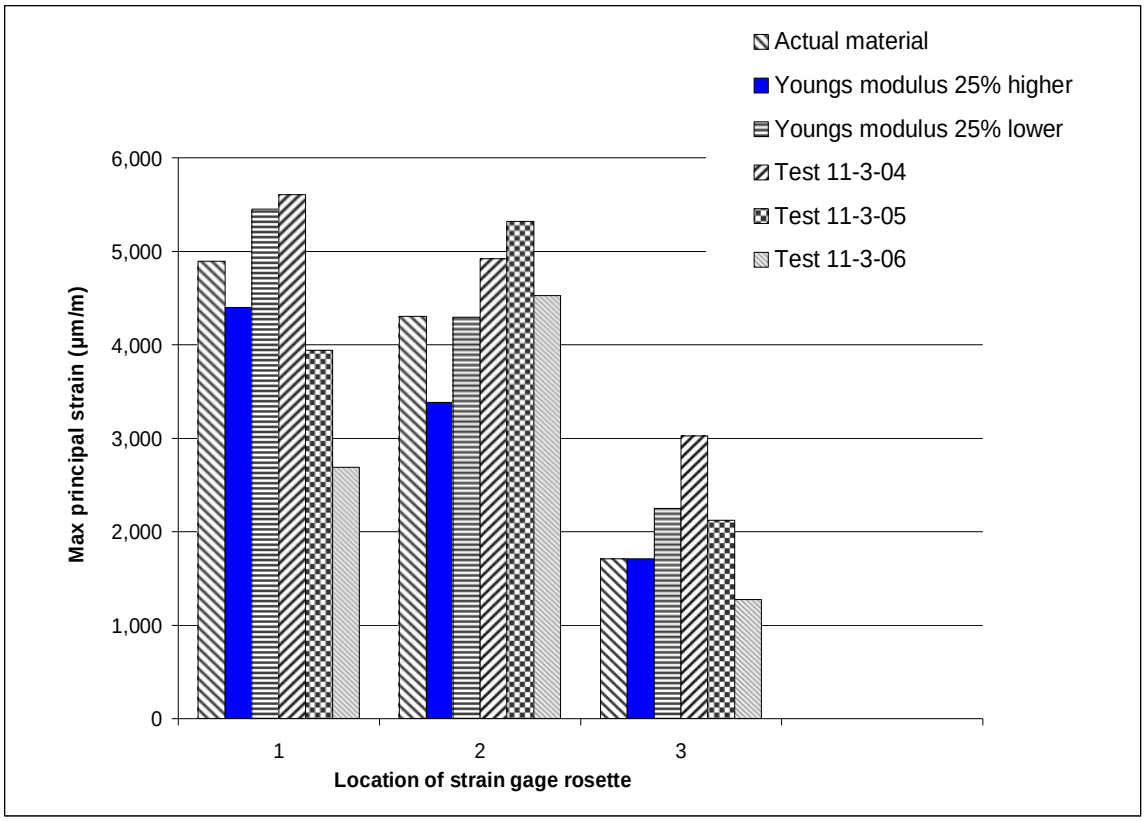

Figure 36. Sensitivity of maximum principal strain at three actual transducer locations.

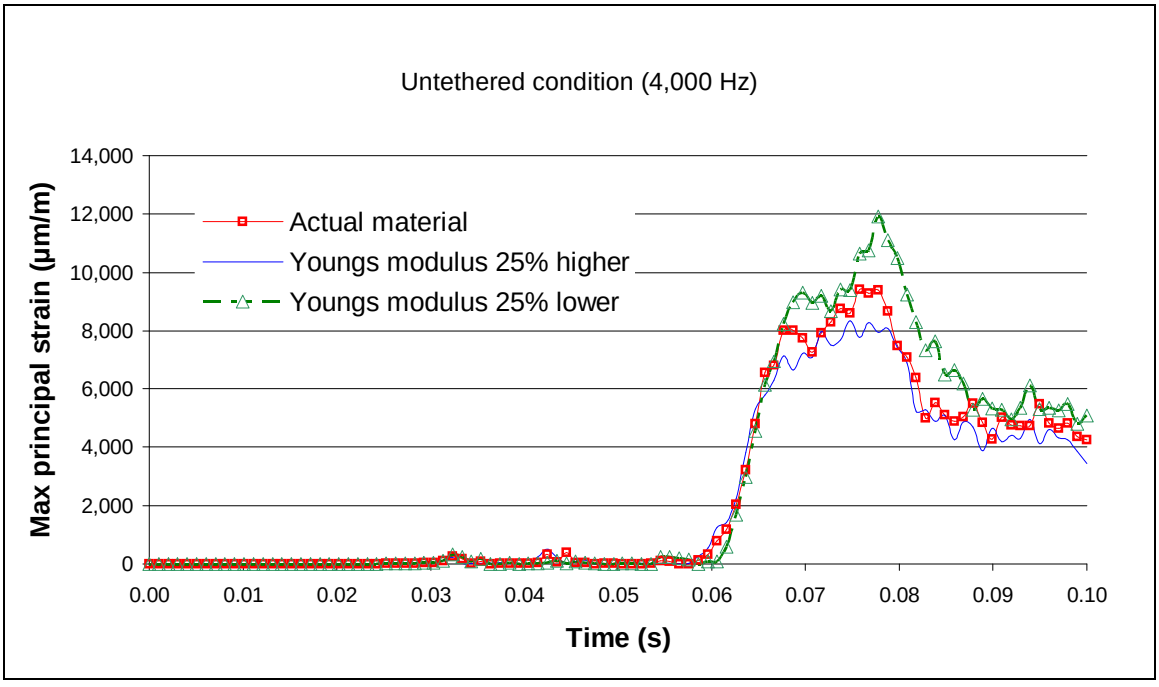

Figure 37. MADYMO-predicted strain as a function of Young's modulus at point 5 in Figure 35.

CONCLUSIONS AND FUTURE WORK

A previously CenTIR-developed provisional MADYMO rigid body/finite element model of a production CRS and its dummy occupant subjected to a modified FMVSS 213 sled test environment was enhanced in an effort to adequately predict the state of strain at any point on the surface of its shell structure. Overall correlation between its principal strain forecasts and those obtained from actual strain gage instrumentation located at five different points on the shell ranged from good to poor.

The model also was exercised as part of a first-approximation type exploratory "what-if" study to evaluate its potential as a decision-making tool for the a priori installation of strain gages that might be employed in future CRS developmental sled testing activities. Several model inadequacies were observed, many of which can be attributed to the use of assumed or best-guess material property inputs. Further investigation using more accurate models will be necessary to obtain more reliable strain forecasts.

A parallel task involved the application of the CenTIR's recently developed state-of-the-art three-dimensional scientific visualization tool, NCVM, to dynamic imagery generated by MADYMO. NCVM demonstrated great promise as (1) a new mechanism by which scientists and engineers can observe the time-varying geometry of a typical CRS/dummy model and thus better understand the relevant physics involved, and (2) as a sled test planning tool.

Future work envisioned with regard to this endeavor is outlined below in the three primary research categories involved: (1) sled testing, (2) computer modeling, and (3) scientific visualization:

- Sled testing: Additional sled tests are planned at General Dynamics to obtain empirical data needed to evaluate the fidelity of future MADYMO models that will most likely be developed and exercised to support NHTSA's planned FMVSS 213 upgrade.

- Computer modeling: CenTIR analysts plan to perform more comprehensive perturbation studies with the small-mesh model to examine the safety-related implications of alternative latch belt anchorage locations, test bench geometry, test bench material compliance properties, and (frontal) sled pulses. In addition, we would like to develop a MADYMO model that can evaluate CRS performance in non-FMVSS 213 type impact configurations (e.g., angled frontal, rear, and side) more typical of real-world vehicular crashes.

- Scientific visualization: Our visualization specialists look to expand the operability of the NCVM to better facilitate and augment the physical sled test results that are currently being modeled and subsequently visualized. For validation purposes, the authors propose to incorporate video data obtained from a sled test directly into the NCVM simulation to create either a side-by-side or an "overlapped" comparison with its virtual counterpart, from a variety of visual perspectives. Clearly, it is here that our newly-added "hot views" feature will be of particular interest. As alluded to earlier, the "vapor trails" option also could be expanded to

provide the capability to not only see the "morphed" image on a single frame, but physically track/plot the displacement of a user-defined location on the dummy geometry.

ACKNOWLEDGEMENTS

The authors would like to thank David P. Roberts, Facility Manager of General Dynamics' HYGE Sled Facility, and his entire sled test team for conscientiously applying their individual and collective expertise on behalf of this research. Alan Blatt of General Dynamics and John Lordi of the University at Buffalo provided valuable advice and guidance throughout the course of this project. We also are indebted to Darryl R. Peterson, Senior Applications Engineer at Vishay Micro-Measurements Group, for his assistance with strain gage selection and application. The authors wish to acknowledge the financial support provided by the Federal Highway Administration (FHWA) and the National Highway Traffic Safety Administration (NHTSA). In addition, Dr. Hulme acknowledges the New York State Assembly for their financial support of NYSCEDII, the research organization under whose auspices the NCVM portion of this work was performed. This project was executed at the Center for Transportation Injury Research (CenTIR) under the direction of the Calspan-UB Research Center, Inc. (CUBRC). The CenTIR is funded by Grant No. DTFH61-98-X-00103 from FHWA to CUBRC.

REFERENCES

[1] Department of Transportation Laboratory Test Procedure # TP-2 13-04, September 1, 1997.

[2] Title 49 CFR: Part 571, Federal Motor Vehicle Safety Standard 213, "Child Restraint Systems."

[3] "Request for an ASME Standard on Verification and Validation in Computational Solid Mechanics," Voting Version 4 July 00, July 2000. On-line Web reference: www.schwer.net/VnV/PDF_Documents/Request-F.pdf.

[4] Oberkampf, W.L., Trucano, T.G., and Hirsch, C., "Verification, Validation, and Predictive Capability in Computational Engineering and Physics," Foundations for Verification and Validation in the 21st Century Workshop, Johns Hopkins University/Applied Physics Laboratory, Laurel, Maryland, October 22-23, 2002.

[5] Knupp, P. and Kambiz, S., *Verification of Computer Codes in Computational Science and Engineering* (New York: Chapman & Hall/CRC, 2003).

[6] Hulme, K., Galganski, R., Patra, A. Vusirikala, N., "A Virtual Prototyping Toolkit for Assessment of Child Restraint System (CRS) Safety," final manuscript submitted for publication in the Proceedings of the SAE 2004 World Congress.

[7] "MADYMO Manuals, Version 5.4, Revision 1.4," TNO Automotive, July, 1999. On-line Web reference: www.MADYMO.com.

[8] Trinca, G.W., and Arnberg, W., "Evaluation of different types of child restraint systems for cars." Accident Analysis & Prevention, Volume 13, Issue 1, March 1981, Pages 11-16.

[9] Rudin-Brown, C.M., Kumagai, J.K., et al., "Usability issues concerning child restraint system harness design." Accident Analysis & Prevention, Volume 35, Issue 3, May 2003, Pages 341-348.

[10] Lefeuve, J., Verron, E., et al., "Numeric simulation of a child restraint seat, Mécanique & Industries." Volume 3, Issue 2, 2002, Pages 201-208.

[11] Carlsson, G. and Ysander, H.N., "Rearward-facing child seats—The safest car restraint for children?" Accident Analysis & Prevention, Volume 23, Issues 2-3, April-June 1991, Pages 175-182.

[12] Arbogast, K., Durbin, D. et al., "An evaluation of the effectiveness of forward facing child restraint systems." Accident Analysis & Prevention, In Press, June, 2003.

[13] Czernakowski, W. and Müller, M., "Misuse mode and effects analysis—An approach to predict and quantify misuse of child restraint systems." Accident Analysis & Prevention, Volume 25, Issue 3, June 1993, Pages 323-333.

[14] Noureddine, A., Eskandarian, A., and Digges, K., "Computer modeling and validation of a hybrid III dummy for crashworthiness simulation." Mathematical and Computer Modeling, Volume 35, Issues 7-8, April 2002, Pages 885-893.

[15] Arlt, F. and Marach, A., "CAD modeling of a human 3D child body." International Journal of Industrial Ergonomics, Volume 22, Issues 4-5, 1 November 1998, Pages 333-341.

[16] Klinich, K.D., Hulbert, G.M., and Schneider, L.W., "Estimating infant head injury criteria and impact response using crash reconstruction and finite element modeling." Stapp Car Crash Journal, Vol. 46, Nov. 2002, p. 165-194. Report No.: SAE 2002-22-0009.

[17] Thacker, J.G., Reagan, S.W., et al., "Experiences during development of a dynamic crash response automobile model." Finite Elements in Analysis and Design, Volume 30, Issue 4, 15 October 1998, Pages 279-295.

[18] Grant, R.H., Brutel, G., et al., "The investigation of accidents involving restrained children as part of the CREST project (Child Restraint System for Cars)." International IRCOBI Conference on the Biomechanics of Impact, Goteborg, Sweden, September, 1998, pp. 73-87.

[19] Kayvantasch, K., "Advanced Technologies for Virtual Testing – A European Approach." 3rd Annual European Vehicle Passive Safety Network Conference, Brussels, Belgium, October, 2002.

[20] Wismans, J., "Integrated Project on Advanced Protective Systems (APROSYS)." European Vehicle Passive safety Network, 2nd Partner's Meeting, Brussels, Belgium, March, 2003.

[21] Hybrid III 3 year old (revision 1.4 of d3hyb33y.dat), in TNO-MADYMO, "Database Manual, Version 5.4." Delft, The Netherlands, July, 1999.

[22] "Hypermesh v5.0 User's Manual", (web link), Altair Engineering. http://www.altair.com/software/hw_hm.htm.

[23] Beier, K.P., "Virtual Reality - Advanced Design and Manufacturing." ESD Technology, Volume 56, No. 1, pp 22-28, January 1995.

[24] Gomes de Sá, A., and Zachmann, G., "Virtual reality as a tool for verification of assembly and maintenance processes." Computers & Graphics, Volume 23, Issue 3, 1 June 1999, Pages 389-403.

[25] Pratt, M.J., "Virtual Prototypes and Product Models in Mechanical Engineering." In: Rix, J., Haas, S., and Teixeira, J., "Virtual Prototyping – Virtual Environments and the Product Design Process." London: Chapman & Hall, 1995: 113-128.

[26] Beier, K.P., "Virtual Reality in Automotive Design and Manufacturing." Proceedings, Convergence '94, International Congress on Transportation Electronics, SAE (Society of Automotive Engineers), Dearborn, Michigan, October 1994.

[27] Woo, M., Neider, J., Davis, T., and Shreiner, D., "OpenGL Programming Guide, Third Edition." Addison-Wesley Publishing, Reading, MA, 2000.

[28] Bourke, P., "Creating Anaglyphs Using OpenGL." On-line web reference: http://astronomy.swin.edu.au/~pbourke/opengl/redblue/, August, 2000.

APPENDIX

The strain gage transducers utilized in this research were EA-06-125RA-120LE planar-construction general-purpose three-element 45-degree rectangular rosettes manufactured by Vishay Micro-Measurements Group (www.vishaymeasurementsgroup.com). They were cemented to the surface of the CRS shell at five locations and connected electrically to the General Dynamics Sled Facility data acquisition system. These gages have a tough, flexible backing and come with preattached, ¾-inch-long copper lead wires coated with polyimide. Overall rosette length and width (the "footprint") are 0.275 and 0.424 inches, respectively.

Numerous application-specific factors were evaluated by experienced Micro-Measurements Group technical representatives before the above selection was made. For example, EA-series gages were recommended because they are flexible enough to be applied to even a slightly curved surface. Their flexibility, however, comes with a trade-off: unprotected grids. As a result, it was necessary to cover them with a coating after installation.

The gages were affixed to the shell following the procedure outlined below:

1.Wash surface with isopropyl alcohol.
2. Sand washed region with 400-grit silicon-carbide paper.
3. Wash surface again with alcohol.
4. Scrub surface with Comet cleanser.
5. Rinse off Comet residue with distilled water.
6. Wipe the area with Neutralizer 5A solution.
7. Glue the gage to the surface.
    - Use AE-10 adhesive.
    - Clamp the gage to the surface (or otherwise maintain constant pressure on it).
    - Allow the adhesive to cure for at least six hours.
8. Coat the top surface of the gage with a very thin layer of AE-10 adhesive.